

Phenomenology of the Hidden $SU(2)$ Vector Dark Matter Model

Nabil Baouche,^{1,2,*} Amine Ahriche,^{3,4,†} Gaber Faisal,^{5,‡} and Salah Nasri^{6,4,§}

¹*Faculty of Science and Technology, University of Jijel PB 98 Ouled Aissa, DZ-18000 Jijel, Algeria.*

²*Laboratoire de Physique des Particules et Physique Statistique,*

Ecole Normale Supérieure, BP 92 Vieux Kouba, DZ-16050 Algiers, Algeria.

³*Department of Applied Physics and Astronomy, University of Sharjah, P.O. Box 27272 Sharjah, UAE.*

⁴*The Abdus Salam International Centre for Theoretical Physics, Strada Costiera 11, I-34014, Trieste, Italy.*

⁵*Department of Physics, Faculty of Arts and Sciences,*

Sueleyman Demirel University, Isparta, Turkey 32260.

⁶*Department of physics, United Arab Emirates University, Al-Ain, UAE.*

We investigate the phenomenology of an extension of the Standard Model (SM) by a non-abelian gauge group $SU(2)_{HS}$ where all SM particles are singlets under this gauge group, and a new scalar representation ϕ that is singlet under SM gauge group and doublet under $SU(2)_{HS}$. In this model, the dark matter (DM) candidates are the three mass degenerate dark photons A_i ($i = 1, 2, 3$) of $SU(2)_{HS}$; and the hidden sector interacts with the (SM) particles through the Higgs portal interactions. Consequently, there will be a new CP-even scalar η that could be either heavier or lighter than the SM-like Higgs. By taking into account all theoretical and experimental constraints such as perturbativity, unitarity, vacuum stability, non-SM Higgs decays, DM direct detection, DM relic density, we found viable DM is possible in the range from GeV to TeV. Within the viable parameters space, the both of the triple Higgs coupling and the di-Higgs production at LHC14 could be enhanced or reduced depending on the scalar mixing and the mass of the scalar particle η .

arXiv:2105.14387v1 [hep-ph] 29 May 2021

* baouche.nabil@gmail.com

† ahriche@sharjah.ac.ae

‡ gaberfaisal@sdu.edu.tr

§ snasri@uaeu.ac.ae

I. INTRODUCTION

It is a fact that 27% of the matter in the universe is made out of cold dark matter (CDM). Historically, its existence was proposed as a possible explanation for several astrophysical observations in the cluster of galaxies [1]. The combined analysis of the Planck satellite 2018 results gives a value of the relic abundance of DM density [2]

$$\Omega_{\text{DM}}h^2 = 0.120 \pm 0.001, \quad (1)$$

where h is the reduced Hubble constant and Ω_{DM} denotes the energy density of DM in unit of the critical density. Obviously, the DM candidate must be a stable particle, or at least its lifetime is much larger than the lifetime of the universe, with no direct interaction with the electroweak and strong forces. Its stability can be guaranteed by imposing an appropriate symmetry, which can be discrete or continuous. In addition, it has also to be non-relativistic, i.e. cold as the possibility of hot dark matter (DM) is ruled out by several observations. Among these observations one can list briefly, the pattern of fluctuations in the cosmic microwave background, the so early formation of stars, galaxies, and clusters of galaxies and the weak lensing signals we observe. Thus one should consider going beyond SM physics for possible DM candidates. In the literature, many extensions of the SM have been proposed with the DM being a scalar [3], fermion [4] or a vector boson [5, 6].

In this work, we consider a model, beyond SM, where DM candidates as a multiplet of massive non-standard spin-1 gauge bosons that interact with the SM through the Higgs portal, which was originally proposed in [6]. This model has the privilege that the stability of the DM particles is guaranteed by the custodial symmetry associated to the gauge symmetry and particle content of the model. This symmetry is favored as one, in this case, does not need to impose any kind of discrete or global symmetry by hand. However, several important features of the model were not investigated due to the non-observation of the Higgs boson at the time of the study. For instances, the measurements of some of the Higgs couplings to a reasonable precision can be used to constrain any heavy scalar state which mixes with the SM-like Higgs boson which will be carried in this work. Additionally, triple Higgs coupling and the Di-Higgs production turn to be so important to shed light on new physics and to understand the electroweak symmetry breaking. All these issues will be investigated in this work. Moreover, we provide the complete explicit analytic expressions of the cross sections of the DM annihilation and co-annihilation different channels that contribute to the thermal relic density at freeze out needed for estimating DM relic density. These expressions were not reported in [6]. Finally, we will report the results related to the branching ratios of several decay modes of the scalars in the model which can be tested in future collider experiments.

The paper is organized as follows. First, we review the model proposed in [6] and discuss the mass eigenstates and their couplings that arise from the scalar potential in section II. Then in section III, we investigate the theoretical and experimental constraints, such as vacuum stability, unitarity, and DM direct detection bound, that can be imposed on the model parameters. In section IV, we consider the lightest gauge vector of the $SU(2)_{HS}$ to be a DM candidate and estimate its relic density by considering all possible allowed annihilation channels as well the coannihilation effects. Next, we carry out a detailed study of the collider phenomenology of the model in section V. Finally, we summarize our results and conclude in section VI. Some relevant formulas and expressions of the effective potential and the cross section contributions are given in Appendix A and Appendix B, respectively.

II. MODEL

In this study, we consider the proposed model in [6]. The model is based on enlarging the gauge symmetry of the SM to include a non-abelian gauge symmetry, is referred to as $SU(2)_{HS}$, under which all SM particles are singlets. The scalar sector of the model contains a new doublet ϕ that is charged under the group $SU(2)_{HS}$ and is singlet under the SM gauge group. The extra gauge bosons, associated to $SU(2)_{HS}$, are denoted by A^μ . They couple to the SM only through the Higgs portal ($-\lambda_m\phi^\dagger\phi H^\dagger H$) and do not mix with the SM gauge bosons due

to the non-abelian character of $SU(2)_{HS}$ [6]. The Lagrangian of the model can be expressed as

$$\mathcal{L} \supset -\frac{1}{4}F^{\mu\nu} \cdot F_{\mu\nu} + (D_\mu\phi)^\dagger(D^\mu\phi) - \lambda_m\phi^\dagger\phi H^\dagger H - \mu_\phi^2\phi^\dagger\phi - \lambda_\phi(\phi^\dagger\phi)^2, \quad (2)$$

where $D^\mu\phi = (\partial^\mu - ig_\phi\frac{\tau_i}{2}A_i^\mu)\phi$ with g_ϕ is the $SU(2)_{HS}$ gauge coupling; and τ_i are the Pauli matrices. The Higgs potential of the SM is parameterized as: $\mathcal{L}^{SM} \supset -\mu^2 H^\dagger H - \lambda(H^\dagger H)^2$ with $H^T = (\chi^+, \frac{1}{\sqrt{2}}[h' + i\chi^0])$. For suitable choice of the parameters μ_ϕ^2 and λ_m , the gauge symmetry $SU(2)_{HS}$ is spontaneously broken when the vacuum expectation value of ϕ , v_ϕ , is not vanishing. After expressing the new doublet in the unitary gauge as

$$\phi = \frac{v_\phi + \eta'}{\sqrt{2}} \exp\left\{-i\tau_k \frac{\zeta_k}{v_\phi}\right\} \begin{pmatrix} 0 \\ 1 \end{pmatrix}, \quad (3)$$

one gets

$$\begin{aligned} \mathcal{L} = & \mathcal{L}_{SM} - \frac{1}{4}F_{\mu\nu} \cdot F^{\mu\nu} + \frac{1}{8}(g_\phi v_\phi)^2 A_\mu \cdot A^\mu + \frac{1}{8}g_\phi^2 A_\mu \cdot A^\mu \eta'^2 + \frac{1}{4}g_\phi^2 v_\phi A_\mu \cdot A^\mu \eta' \\ & + \frac{1}{2}(\partial_\mu \eta')^2 - \frac{\lambda_m}{2}(\eta' + v_\phi)^2 H^\dagger H - \frac{\mu_\phi^2}{2}(\eta' + v_\phi)^2 - \frac{\lambda_\phi}{4}(\eta' + v_\phi)^4, \end{aligned} \quad (4)$$

where $A_\mu = UA'_\mu U^{-1} - \frac{i}{g_\phi}[\partial_\mu U]U^{-1}$ with $U = \exp\{-i\tau_k \zeta_k / v_\phi\} \in SU(2)_{HS}$. In the A_i^μ component space, the Lagrangian \mathcal{L} in (4) has $SO(3)$ custodial symmetry. As a consequence, the three A_i^μ components are degenerate in mass, $m_A = g_\phi v_\phi / 2$, stable and hence can serve as vector DM candidates.

In order to proceed, we need to express \mathcal{L} in (4) in terms of the mass eigenstates. This can be done after minimizing the scalar potential along both ϕ and H directions. Setting $H = \exp\{-i\tau_k \chi_k / v\} \cdot (0, \frac{1}{\sqrt{2}}[v + h'])^T$, where $v = 246 \text{ GeV}$ is the usual Higgs vacuum expectation value. By imposing the tadpole conditions $\partial V / \partial h = \partial V / \partial \eta = 0$ one finds

$$\mu^2 = -\lambda v^2 - \frac{1}{2}\lambda_m v_\phi^2, \quad \mu_\phi^2 = -\lambda_\phi v_\phi^2 - \frac{1}{2}\lambda_m v^2. \quad (5)$$

The h' - η' mixing due to the presence of the term of λ_m in (4), leads to the mass squared matrix

$$M^2 = \begin{pmatrix} 2\lambda v^2 & \lambda_m v v_\phi \\ \lambda_m v v_\phi & 2\lambda_\phi v_\phi^2 \end{pmatrix}, \quad (6)$$

which gives the eigenvalues and the mixing

$$m_{1,2}^2 = \lambda v^2 + \lambda_\phi v_\phi^2 \mp \sqrt{(\lambda v^2 - \lambda_\phi v_\phi^2)^2 + \lambda_m^2 v^2 v_\phi^2}, \quad t_{2\beta} = \frac{\lambda_m v v_\phi}{\lambda_\phi v_\phi^2 - \lambda v^2}, \quad (7)$$

where $t_{2\beta} = \tan 2\beta$. By diagonalizing M^2 , we get the mass eigenstates h and η that are defined as

$$\begin{pmatrix} h \\ \eta \end{pmatrix} = \begin{pmatrix} c_\beta & -s_\beta \\ s_\beta & c_\beta \end{pmatrix} \begin{pmatrix} h' \\ \eta' \end{pmatrix}, \quad (8)$$

with $c_\beta = \cos \beta$, $s_\beta = \sin \beta$. Since the couplings are real, the eigenvalues of the matrix M^2 are required to be positive definite only if

$$\lambda > 0, \quad \lambda_\phi > 0, \quad 2\lambda_m + \sqrt{\lambda\lambda_\phi} > 0. \quad (9)$$

In our analysis, we identify the $m_h \sim 125 \text{ GeV}$ eigenstate to be the SM-like Higgs boson and η the other eigenstate, therefore, we have two cases where the SM-like Higgs eigenstate is the (1) light or the (2) heavy eigenstate. Then, in the first case, the CP-even scalar masses (7) should be written as

$$m_{h,\eta}^2 = \lambda v^2 + \lambda_\phi v_\phi^2 \mp (\lambda_\phi v_\phi^2 - \lambda v^2) / c_{2\beta}, \quad (10)$$

with $c_{2\beta} = \cos 2\beta$ and the quartic couplings can be expressed as

$$\lambda = \frac{m_h^2}{2v^2} c_\beta^2 + \frac{m_\eta^2}{2v^2} s_\beta^2, \quad \lambda_\phi = \frac{m_h^2}{2v_\phi^2} s_\beta^2 + \frac{m_\eta^2}{2v_\phi^2} c_\beta^2, \quad \lambda_m = \frac{s_{2\beta}}{2vv_\phi} (m_\eta^2 - m_h^2). \quad (11)$$

In the second case, the CP-even scalar masses are given by (7) are

$$m_{h,\eta}^2 = \lambda v^2 + \lambda_\phi v_\phi^2 \pm (\lambda_\phi v_\phi^2 - \lambda v^2) / c_{2\beta}, \quad (12)$$

and the quartic couplings

$$\lambda = \frac{m_h^2}{2v^2} s_\beta^2 + \frac{m_\eta^2}{2v^2} c_\beta^2, \quad \lambda_\phi = \frac{m_h^2}{2v_\phi^2} c_\beta^2 + \frac{m_\eta^2}{2v_\phi^2} s_\beta^2, \quad \lambda_m = \frac{s_{2\beta}}{2vv_\phi} (m_h^2 - m_\eta^2). \quad (13)$$

Clearly, the model can be described by the four free parameters g_ϕ , λ_ϕ , μ_ϕ and λ_m , or equivalently by s_β , g_ϕ , m_η and v_ϕ , in addition to the SM parameters.

Keeping only terms relevant to our study, in the Lagrangian in the mass eigenstates basis, we can write

$$\begin{aligned} \mathcal{L} \supset & -\frac{1}{4} F_{\mu\nu} \cdot F^{\mu\nu} + \frac{1}{2} m_A^2 A_\mu \cdot A^\mu - \frac{1}{2} m_\eta^2 \eta^2 - \frac{1}{2} m_h^2 h^2 - (h c_\beta + \eta s_\beta) \left(\sum_f \frac{m_f}{v} f \bar{f} \right) \\ & + \left[\frac{s_\beta^2}{2v} \eta^2 + \frac{c_\beta^2}{2v} h^2 + \frac{s_{2\beta}}{2v} \eta h + \eta s_\beta + h c_\beta \right] \left(\frac{2m_W^2}{v} W_\mu^+ W^{-\mu} + \frac{m_Z^2}{v} Z^\mu Z_\mu \right) \\ & + \left[\frac{c_\beta^2}{2v_\phi} \eta^2 + \frac{s_\beta^2}{2v_\phi} h^2 - \frac{s_{2\beta}}{2v_\phi} \eta h + \eta c_\beta - h s_\beta \right] \left(\frac{m_A^2}{v_\phi} A_\mu \cdot A^\mu \right) \\ & - \frac{1}{6} \rho_h h^3 - \frac{1}{6} \rho_\eta \eta^3 - \frac{1}{2} \rho_1 \eta^2 h - \frac{1}{2} \rho_2 h^2 \eta. \end{aligned} \quad (14)$$

where f denotes the SM fermions and the ρ 's parameters represents the CP-even scalar triple couplings that are given by

$$\begin{aligned} \rho_1 &= -6\lambda_\phi v_\phi c_\beta^2 s_\beta + 6\lambda v s_\beta^2 c_\beta + \lambda_m (v c_\beta^3 - v_\phi s_\beta^3 - 2v c_\beta s_\beta^2 + 2v_\phi c_\beta^2 s_\beta), \\ \rho_2 &= 6\lambda_\phi v_\phi s_\beta^2 c_\beta + 6\lambda v c_\beta^2 s_\beta + \lambda_m (v s_\beta^3 + v_\phi c_\beta^3 - 2v c_\beta^2 s_\beta - 2v_\phi s_\beta^2 c_\beta), \\ \rho_\eta &= 6\lambda_\phi v_\phi c_\beta^3 + 6\lambda v s_\beta^3 + 3\lambda_m c_\beta s_\beta (v c_\beta + v_\phi s_\beta), \\ \rho_h &= -6\lambda_\phi v_\phi s_\beta^3 + 6\lambda v c_\beta^3 + 3\lambda_m c_\beta s_\beta (v s_\beta - v_\phi c_\beta). \end{aligned} \quad (15)$$

We notice from (14), that the couplings of h and η to SM particles are weighted by c_β and s_β , respectively. Moreover, in the first case the scalar η can additionally decay into Higgs pairs if $m_\eta > 2m_h$ with the partial decay width

$$\Gamma(\eta \rightarrow hh) = \Theta(m_\eta - 2m_h) \frac{\rho_2^2}{32\pi m_\eta} \sqrt{1 - 4 \frac{m_h^2}{m_\eta^2}}, \quad (16)$$

and in the second case, the Higgs can decay into a pair of η if $m_h > 2m_\eta$, in addition to their possible decay to $A_i A_i$.

III. THEORETICAL & EXPERIMENTAL CONSTRAINTS

This model is subject to a number of theoretical and experimental constraints such as vacuum stability, perturbativity, perturbative unitarity, electroweak precision tests (EWPT), and the constraints from the Higgs decay. For the EWPT, it is expected that the new physics contribution to the oblique parameters (ΔS and ΔT)

is negligible since the scalar doublet η is a singlet the SM gauge group. Then, by considering the constraints from the Higgs signal strength $\mu_{\text{tot}} \geq 0.89$ at 95% CL [7], the $h - \eta$ mixing makes both ΔS and ΔT very tiny, and all the space parameters will be allowed by the EWPT. In what follows, we discuss the above mentioned constraints in details.

- **Unitarity constraints**

Possible constraints on the quartic couplings λ , λ_ϕ and λ_m , can be derived upon requiring that the amplitudes for the scalar-scalar scattering $S_1 S_2 \rightarrow S_3 S_4$ at high energies respect the tree-level unitarity [8]. Here, S_i can be h or η for $i = 1, 2, 3, 4$. This can be understood as, at high energies, the dominant contributions to these amplitudes are those mediated by the quartic couplings [9]. Denoting the eigenvalues of the scattering matrix as Λ_i , the unitarity condition reads

$$|\Lambda_i| \leq 8\pi \quad (17)$$

In the model under concern the above bound results in the following constraints

$$\lambda_m \leq 8\pi, \quad \lambda \leq 4\pi, \quad \lambda_\phi \leq 4\pi, \quad 3(\lambda + \lambda_\phi) \pm \sqrt{9(\lambda - \lambda_\phi)^2 + 4\lambda_m^2} \leq 8\pi. \quad (18)$$

- **Vacuum Stability and Perturbativity**

The quartic couplings of the scalar potential is subjected to a number of constraints to ensure that the potential is bounded from below and that the couplings remain perturbative as well the electroweak vacuum to be stable all the way up to the Planck scale. For the scalar potential to be bounded from below, the conditions $\lambda > 0$, $\lambda_\phi > 0$ and $\lambda\lambda_\phi > 0$ must hold and for the case $\lambda_m < 0$, the condition $2\lambda_m + \sqrt{\lambda\lambda_\phi} > 0$ must be also satisfied. Recall that, one needs $4\lambda\lambda_\phi > \lambda_m^2$ so that the Higgs mixing matrix M^2 is positive definite and thus $m_h, m_\eta > 0$.

- **Constraints on the Higgs Decays**

Since the Higgs couplings are modified in our model, and since there exist new particles with new interactions, then the Higgs total decay width and branching ratios get modified. Here, all the vertex of the Higgs-gauge fields and Higgs-fermions are scaled by c_β , therefore the Higgs partial decay widths to the SM particles are scaled as $\Gamma(h \rightarrow X_{SM} \bar{X}_{SM}) = c_\beta^2 \Gamma_{SM}(h \rightarrow X_{SM} \bar{X}_{SM})$. In addition to the SM final states, the Higgs may decay into new gauge bosons (dark photons) if kinematically allowed, with the Higgs partial decay width

$$\Gamma_{inv}(h \rightarrow AA) = \sum_{i=1}^3 \Gamma(h \rightarrow A_i A_i) = 3\Theta(m_h - 2m_A) \frac{g_\phi^2 m_h^3 s_\beta^2}{64\pi m_A^2} \sqrt{1 - 4\frac{m_A^2}{m_h^2}} \left\{ 1 - 4\frac{m_A^2}{m_h^2} + 12\frac{m_A^4}{m_h^4} \right\}, \quad (19)$$

this channel is open when $m_A < m_h/2$. The factor "3" in (19) refers to the summation over $A_i A_i$. In Case 2 where the condition $m_h > 2m_\eta$ may be fulfilled, the decay channel $h \rightarrow \eta\eta$ is open and the partial width is given by

$$\Gamma(h \rightarrow \eta\eta) = \Theta(m_h - 2m_\eta) \frac{\rho_1^2}{32\pi m_h} \sqrt{1 - 4\frac{m_\eta^2}{m_h^2}}. \quad (20)$$

Therefore, the Higgs total decay width can be written as

$$\Gamma_h = \Gamma_{BSM} + c_\beta^2 \Gamma_h^{SM}, \quad (21)$$

where $\Gamma_h^{SM} = 4.2$ MeV is the Higgs total decay width in the SM; $\Gamma_{BSM} = \Gamma_{inv}$ for Case 1; and $\Gamma_{BSM} = \Gamma_{inv} + \Gamma_{und}$ for Case 2. Here, the undetermined Higgs decay width $\Gamma_{und} = \Gamma(h \rightarrow \eta\eta)$, which is different than the invisible one at collider; since the light scalar can be seen at detector via the decay to light

fermions $\eta \rightarrow f\bar{f}$. These decays do not match the known SM ones, hence, the signal $h \rightarrow \eta\eta \rightarrow f_1\bar{f}_1f_2\bar{f}_2$ is named untermind. Then, the invisible and undetermined branching ratio must respect the constraints [10, 11]¹

$$\mathcal{B}_{inv} < 0.26, \mathcal{B}_{und} < 0.22, \mathcal{B}_{inv} + \mathcal{B}_{und} \leq 0.47. \quad (22)$$

In addition, the Higgs total decay width should lie in the range [14, 15]

$$1.0 \text{ MeV} < \Gamma_h < 6.0 \text{ MeV}. \quad (23)$$

• DM Direct Detection Constraints

The DM candidate can interact with nucleons via t -channel diagrams that are mediated by h and η as shown in Fig. 1.

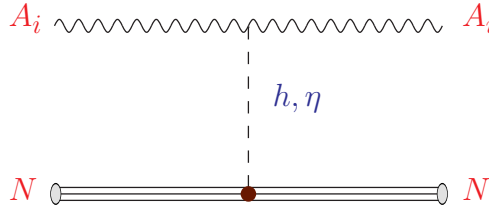


FIG. 1: Feynman diagrams that lead to DM direct detection at underground detectors.

Measuring nuclear recoil energy resulting from the elastic scattering of DM particle off nucleus in detector can serve as a direct search of DM particles. The results of such searches can be used to impose constraints on the relevant parameters of the model. At tree-level, the spin independent elastic scattering of the vector DM off nucleus, mediated by h or η exchange, given in [6], can be simplified as

$$\begin{aligned} \sigma_{SI}(NA \rightarrow NA) &= \frac{1}{64\pi} f^2 g_\phi^4 s_{2\beta}^2 m_N^2 \frac{v_\phi^2 (m_h^2 - m_\eta^2)^2}{v^2 m_h^4 m_\eta^4} \left(\frac{m_N}{m_N + m_A} \right)^2 \\ &= 6.45765608 \times 10^{-42} \text{ cm}^2 s_{2\beta}^2 \left(\frac{g_\phi}{0.5} \right)^4 \left(\frac{v_\phi}{100 \text{ GeV}} \right)^2 \left(\frac{m_h}{m_\eta} \right)^4 \left(1 - \frac{m_\eta^2}{m_h^2} \right)^2 \left(1 + \frac{m_A}{m_N} \right)^{-2}. \end{aligned} \quad (24)$$

Here, m_N denotes the nucleon mass and $f = 0.3$ [6], parametrizes the Higgs nucleon coupling. This has to be compared with the present experimental upper bound on this cross section [16].

• Renormalization Group Equation

The constraints from vacuum stability and couplings perturbativity can be determined by the renormalisation group evolution of $\lambda, \lambda_m, \lambda_\phi$. At one-loop β functions and upon neglecting all the Yukawa couplings except for y_t , the relevant equations are given as [7, 17]:

$$\begin{aligned} 16\pi^2 d\lambda/dt &= 24\lambda^2 + 2\lambda_m^2 - 6y_t^4 + \lambda(12y_t^2 - \frac{9}{5}g_1^2 - 9g_2^2) + \frac{27}{200}g_1^4 + \frac{9}{20}g_1^2g_2^2 + \frac{9}{8}g_2^4, \\ 16\pi^2 d\lambda_\phi/dt &= 24\lambda_\phi^2 + 2\lambda_m^2 - 9\lambda_\phi g_\phi^2 + \frac{9}{4}g_\phi^4, \\ 16\pi^2 d\lambda_m/dt &= \lambda_m(6y_t^2 + 12\lambda + 12\lambda_\phi + 4\lambda_m - \frac{9}{10}g_1^2 - \frac{9}{2}g_2^2 - \frac{9}{2}g_\phi^2), \\ 16\pi^2 dg_i/dt &= b_i g_i^3 \quad \text{with } (b_1, b_2, b_3, b_\phi) = (41/6, -19/6, -7, -43/6), \\ 16\pi^2 d\lambda_t/dt &= y_t \left(\frac{9}{2}y_t^2 - \frac{17}{20}g_1^2 - \frac{9}{4}g_2^2 - 8g_3^2 \right), \end{aligned} \quad (25)$$

¹ Recent measurements by ATLAS [12] and CMS [13] of the invisible decay width of the SM Higgs boson give $\mathcal{B}_{inv} < 0.11$ and $\mathcal{B}_{inv} < 0.19$, respectively. In our numerical scan, we will consider the recent ATLAS bound.

where $g_i = (g_1, g_2, g_3)$ represent the SM gauge couplings and g_ϕ is the gauge coupling of the new $SU(2)_H$. In what follows, we will use (25) to check whether the conditions of the vacuum stability, perurbativity and unitarity are fulfilled at higher scales $\Lambda = 100 \text{ TeV}$, 10^4 TeV and $\Lambda = m_{\text{Planck}}$.

IV. DARK MATTER RELIC DENSITY

In order to estimate the relic density, one has to estimate the freeze-out temperature and the annihilation cross section. The thermal relic density at freeze out is given in the terms of the thermally averaged annihilation cross section by [18]:

$$\Omega_{DM} h^2 \simeq \frac{1.04 \times 10^9}{M_{pl}} \frac{x_F}{\sqrt{g_*(x_F)}} \frac{3}{\langle \sigma(AA)v_r \rangle}, \quad (26)$$

where v_r is the relative velocity, $M_{pl} = 1.22 \times 10^{19} \text{ GeV}$ is the Plank mass, g_* counts the total number of relativistic degrees of freedom, and $x_F = m_A/T_f$ is the inverse freeze-out temperature. The factor “3” in (26) comes from the fact that the total relic density is the summation of the contributions of the three vector bosons A_i , that have same masses, same interactions, and hence give the same contribution to the relic density. The total thermally averaged annihilation cross section

$$\langle \sigma(AA)v_r \rangle = \frac{1}{8T m_A^4 K_2^2(m_A/T)} \sum_X \int_{4m_A^2}^{\infty} ds \sigma_{AA \rightarrow X}(s) \sqrt{s} (s - 4m_A^2) K_1(\sqrt{s}/T), \quad (27)$$

where $K_{1,2}$ are the modified Bessel functions and $\sigma_{AA \rightarrow X}(s)$ is the annihilation cross section due to the channel $AA \rightarrow X$, at the CM energy \sqrt{s} .

The freeze-out parameter x_F can be obtained iteratively from the equation:

$$x_F = \log \left(\frac{5}{4} \sqrt{\frac{45}{8}} \frac{3}{2\pi^3} \frac{M_{pl} m_A \langle \sigma(AA)v_r \rangle}{\sqrt{g_*(x_F)} x_F} \right), \quad (28)$$

where the factor “3” in (28) refers to the DM degrees of freedom.

In case where the DM candidate is close in mass to other species, the coannihilation effect becomes important, and in order to take it into account, the thermal average cross section, $\langle \sigma(AA)v_r \rangle$, in (26) and (28) should be replaced the effective one $\langle \sigma_{eff}(AA)v_r \rangle$. The effective thermally averaged annihilation cross section is given by [18]:

$$\begin{aligned} \sigma_{eff}(x) &= \sum_{ij}^N \frac{g_i g_j}{g_{eff}^2} \sigma_{ij} (1 + \Delta_i)^{3/2} (1 + \Delta_j)^{3/2} \exp[-x(\Delta_i + \Delta_j)], \\ g_{eff}(x) &= \sum_{i=1}^N g_i (1 + \Delta_i) \exp(-x\Delta_i), \end{aligned} \quad (29)$$

where $\Delta_i = \frac{m_i - m_{DM}}{m_{DM}}$ and g_i is the multiplicity if the species “ i ”. In our model, we consider the co-annihilation effect coming from the mass degeneracy between the vector bosons A_i , and therefore $g_i = 3$, $g_{eff} = 3$, $\sigma(A_i A_{j \neq i}) = \sigma(A_1 A_2)$ and $\sigma(A_i A_i) = \sigma(A_1 A_1)$. Thus, the effective thermally averaged cross section reads:

$$\sigma_{eff}(AA) = \frac{1}{3} [\sigma(A_1 A_1 \rightarrow \text{all}) + 2\sigma(A_1 A_2 \rightarrow \text{all})]. \quad (30)$$

In our analysis, we estimate the relic density by considering (26), (28) and (30), and confront it to the recent precise measurements from the PLANCK satellite shown in (1). Here, we consider 3σ range, i.e., $0.117 \leq \Omega_{DM} h^2 \leq 0.123$. In the rest of this section, we estimate the different contributions to the cross sections $\sigma(A_1 A_1)$ and $\sigma(A_1 A_2)$.

For the cross section $\sigma(A_1 A_1)$, we have many channels: $f\bar{f}$, WW , ZZ , hh , $\eta\eta$ and $h\eta$ as shown in Fig. 2.

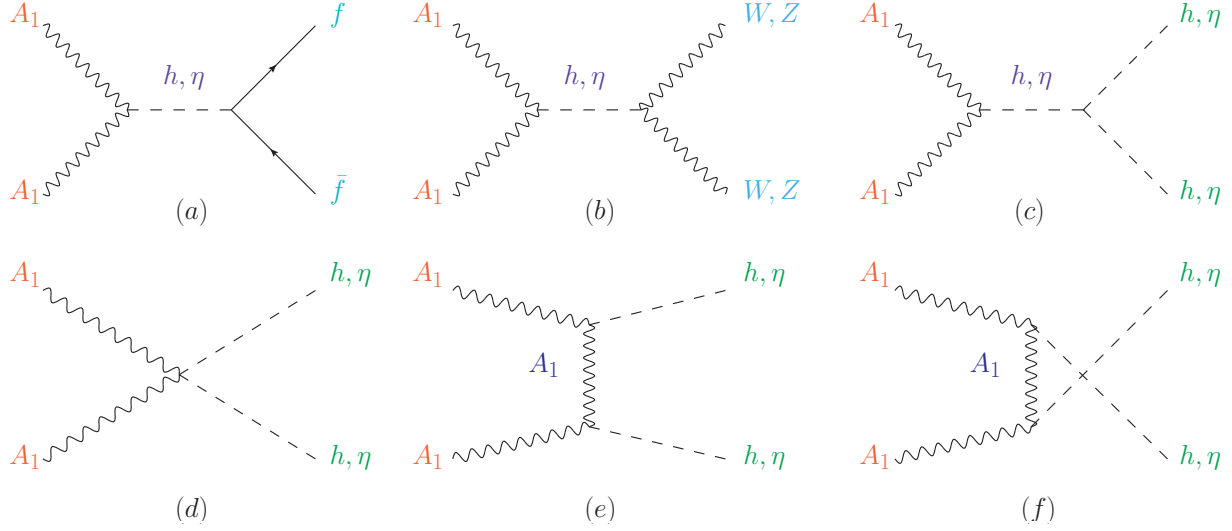


FIG. 2: Different DM self-annihilation channels.

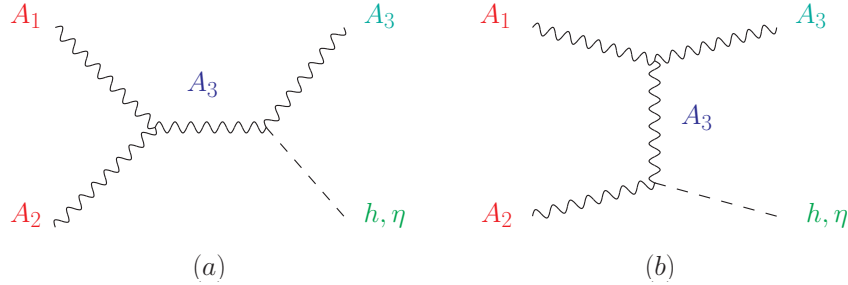


FIG. 3: The DM co-annihilation channel.

While, for the cross section $\sigma(A_1A_2)$, we have only one channel as shown in Fig. 3.

From the diagram in Fig. 2-a, the annihilation cross section into fermion pairs ($f\bar{f}$) at CM energy \sqrt{s} is estimated to be

$$\sigma(A_1A_1 \rightarrow b\bar{f}\bar{f})v_r = N_c \frac{s_{2\beta}^2 m_A^4 m_f^2}{144\pi v_\phi^2 v^2} \mathcal{BW} \left(1 - \frac{4m_f^2}{s}\right)^{\frac{3}{2}} \left(12 - 4\frac{s}{m_A^2} + \frac{s^2}{m_A^4}\right), \quad (31)$$

$$\mathcal{BW} = \left| \frac{i}{s - m_h^2 + im_h\Gamma_h} - \frac{i}{s - m_\eta^2 + im_\eta\Gamma_\eta} \right|^2, \quad (32)$$

with $s_{2\beta} = \sin(2\beta)$, N_c is the color factor (1 for leptons and 3 for quarks), Γ_h (Γ_η) is the total decay width of the Higgs (scalar η).

The annihilation cross section into gauge bosons $V = W, Z$ as shown in Fig. 2-b is found at CM energy \sqrt{s} to be

$$\begin{aligned} \sigma(A_1A_1 \rightarrow VV)v_r &= \delta_V \frac{s_{2\beta}^2 m_A^4 m_V^4}{288\pi s v^2 v_\phi^2} \mathcal{BW} \left(1 - \frac{4m_V^2}{s}\right)^{1/2} \left(12 - 4\frac{s}{m_A^2} + \frac{s^2}{m_A^4}\right) \\ &\times \left(12 - 4\frac{s}{m_V^2} + \frac{s^2}{m_V^4}\right), \end{aligned} \quad (33)$$

where V stands for W^\pm or Z bosons; and $\delta_W = 2$ and $\delta_Z = 1$.

In order to estimate the cross section for the processes $A_1A_1 \rightarrow X \equiv hh, \eta\eta$; we estimated the amplitude by considering the diagrams in Fig. 2-c, Fig. 2-d, Fig. 2-e and Fig. 2-f; and write its averaged squared in powers of

$t - m_A^2$ and $u - m_A^2$, as

$$|\bar{\mathcal{M}}|^2 = \frac{1}{2} \left\{ \frac{Q_1 m_A^4}{(t - m_A^2)^2} + \frac{Q_2 m_A^2}{t - m_A^2} + Q_3 + \frac{Q_4}{m_A^2} (t - m_A^2) + \frac{Q_5}{m_A^4} (t - m_A^2)^2 + \frac{Q_6}{m_A^6} (t - m_A^2)^3 \right\} + \{t \rightarrow u\}. \quad (34)$$

Then, the integration over the angles of the t -terms and u -terms in (34) leads to identical contributions, where the cross section can be presented as

$$\sigma_{\nu r} = \frac{Q_0}{s} \left\{ \frac{2Q_1}{A^2 - B^2} + \frac{Q_2}{B} \ln \left(\frac{A + B}{A - B} \right) + 2Q_3 + 2Q_4 A + \frac{2}{3} Q_5 (3A^2 + B^2) + 2Q_6 A (A^2 + B^2) \right\}, \quad (35)$$

where the dimensionless parameters Q_i , A and B are given in Appendix B. For the processes $A_1 A_1 \rightarrow X \equiv h\eta$ (i.e., diagrams in Fig. 2-c, Fig. 2-d and Fig. 2-e); and $A_1 A_2 \rightarrow X \equiv A_3 h, A_3 \eta$ (i.e., diagrams in Fig. 3); the averaged squared amplitude can be written only in powers of $t - m_A^2$, i.e.,

$$|\bar{\mathcal{M}}|^2 = \frac{Q_1 m_A^4}{(t - m_A^2)^2} + \frac{Q_2 m_A^2}{t - m_A^2} + Q_3 + \frac{Q_4}{m_A^2} (t - m_A^2) + \frac{Q_5}{m_A^4} (t - m_A^2)^2 + \frac{Q_6}{m_A^6} (t - m_A^2)^3, \quad (36)$$

and after integration we get the cross section that has the form (35). The dimensionless parameters Q_i , A and B for the processes $A_1 A_1 \rightarrow X \equiv h\eta$; and $A_1 A_2 \rightarrow X \equiv A_3 h, A_3 \eta$ are also given in Appendix B.

V. COLLIDERS PHENOMENOLOGY

A. Collider Constraints & the Parameters Space

In model under consideration, we have only four free parameters. It is convenient to choose them as: the mass of the DM, m_A , the mass of the new scalar, m_η , the gauge coupling g_ϕ and finally sine of the mixing angle s_β . In our analysis, we perform a numerical scan over the parameters space in the ranges given as

$$|s_\beta| \leq 1, g_\phi \leq \sqrt{4\pi}, m_A, m_\eta \leq 3 \text{ TeV}. \quad (37)$$

These ranges of the parameters space are subjected to the constraints of vacuum stability (9), perturbativity (at the weak scale), unitarity (18), Higgs decay (22) and (23), DM relic density (26), DM direct detection (24); in addition to the collider constraints on the Higgs signal strength (40).

At the LHC, ATLAS and CMS experiments have observed the Higgs boson in several decay channels, mainly $h \rightarrow ZZ, WW, \gamma\gamma, \tau\tau, b\bar{b}$ [19]. The observation allowed both collaborations to measure some of the Higgs couplings to a reasonable precision [19]. In return, these measurements can be used to constrain any heavy scalar state which mixes with the SM-like Higgs boson. The desired constraints can be deduced using the data of the signal strength modifier μ_{XX} for a given search channel, $h \rightarrow XX$. The signal strength modifier is a measured experimental quantity for the combined production and decay and is defined as the ratio of the measured Higgs boson rate to its SM prediction [7, 19]

$$\mu_{XX} = \sigma(pp \rightarrow h \rightarrow XX) / \sigma(pp \rightarrow h \rightarrow XX)|_{\text{SM}}, \quad (38)$$

in the narrow width approximation, μ_{XX} takes the simple form as

$$\mu_{XX} = \frac{\sigma(pp \rightarrow h) \times \mathcal{B}(h \rightarrow XX)}{\sigma(pp \rightarrow h)|_{\text{SM}} \times \mathcal{B}(h \rightarrow XX)|_{\text{SM}}}. \quad (39)$$

As mentioned above, due to the Higgs mixing, the couplings of the observed h_{125} boson to SM fermions and gauge bosons are modified with respect to the SM, by c_β . So, by considering the definitions of the Higgs decay width in (21), one can simplify signal strength modifier as

$$\mu_{XX} = c_\beta^2 (1 - \mathcal{B}_{BSM}), \quad (40)$$

where $\mathcal{B}_{BSM} = \mathcal{B}_{inv}$ for the case $m_\eta > m_h/2$, and $\mathcal{B}_{BSM} = \mathcal{B}_{inv} + \mathcal{B}_{und}$ for $m_\eta < m_h/2$. Thus, the measurement of μ_{XX} of the h_{125} Higgs boson can be used to derive a strong constraint on the mixing angle β and the exotic Higgs decay fraction. The constraints in (40) are complementary to those on the exotic Higgs decays shown in (22) and (23).

The ATLAS and CMS collaborations have presented the results of μ_{XX} for the various final states at the Run-I of the LHC. The LHC Run-I corresponds to $\sqrt{s} = 7$ and $\sqrt{s} = 8$ TeV with the integrated luminosity $5 fb^{-1}$ and $20 fb^{-1}$, respectively. The combined results have been reported in [19]. Based on the reported result of the combined total signal strengths of the h_{125} Higgs, with all production and decay channels combined, one obtains

$$\mu_{tot} \geq 0.89, \quad (41)$$

at 95%CL [7]. This can be translated into a bound on the Higgs mixing angle β that reads $s_\beta^2 \leq 0.11$ in the absence of exotic Higgs decays, i.e., $\mathcal{B}_{BSM} = 0$. Within the LHC Run-II at $\sqrt{s} = 13$ TeV, ATLAS and CMS collaborations reported more accurate results in some decay channels. For instances, observations at 5σ have been achieved in the $b\bar{b}$ mode [20, 21]. The combined results of μ_{XX} at $\sqrt{s} = 13$ TeV have been reported by CMS collaboration in [22], and by ATLAS collaboration in [10]. Unfortunately, a global combination of their obtained results for LHC Run-II was not yet performed. Finally, with more improvement of the experimental sensitivity on the Higgs signal strengths in the future, a more stringent bound $s_\beta < 0.18$ is expected to be reached at the high luminosity LHC in case of $\mathcal{B}_{BSM} = 0$ [23, 24]. For the scenario $m_\eta > m_h$, the results of the direct searches at the LHC, which have been performed by the ATLAS and CMS collaborations, of heavy Higgs decays into $ZZ, WW, \gamma\gamma, hh, t\bar{t}$ can set additional complementary constraints. In particular, the constraints will be imposed on m_η and $|s_\beta|$. For detailed discussion about these constraints we refer to [7] where detailed study and analysis have been performed.

In what follows, we will show the results of our numerical scan by considering all the above aforementioned constraints. For instance, in Fig. 4, we present the viable parameters space among the intervals (37). In Fig. 5, the signal strength (39) is presented versus the total decay width of the new scalar (Γ_η), and the DM observables are presented in Fig. 6.

In the top-left, top-right and bottom-left of Fig. 4, we show the viable $m_\eta - m_A$ space parameters, respecting the aforementioned constraints in the ranges listed in (37), where the palettes show the scalar mixing (top-left), the new scalar vev v_ϕ (top-right); and the new gauge coupling g_ϕ (bottom-left). One notices the existence of three distinct sub-regions in the $m_\eta - m_A$ plan, corresponding to (1) $m_\eta < m_A$, and it is the largest sub-region, (2) $m_\eta \gtrsim 2m_A$, and (3) $m_A \lesssim m_h/2$. Moreover, we remark that the constraints imposed on the parameters space can be easily evaded for values of m_η and m_A close to or larger than the electroweak scale, mostly in the top-right region in each plot, for the preferred ranges of the other parameters given as $|s_\beta| \lesssim 0.1$, $v_\phi \gtrsim 10^3$ and large values of $g_\phi \gtrsim 0.1$. One has to mention that most of the non-viable parameters space (empty regions in Fig. 4-top-right for example) are excluded mainly by DM direct detection and relic density requirements.

Recall that in setup, the new physics contribution to the oblique parameters ΔS and ΔT has negligible effect. As a consequence, having small values of s_β (within the condition (41)) allows to have values m_η close to or larger than the electroweak scale without violating the constraints imposed on ΔS and ΔT . On the other hand, DM direct detection constraints given in (24), can be respected for large values of DM masses. Concerning the DM mass, that is given $m_A = g_\phi v_\phi / 2$, having a small values of g_ϕ can be compensated by large values v_ϕ to get the desired values of m_A that explain the parameters space in Fig. 4. One remarks that the scalar mixing is almost suppressed except in the regions around the degeneracies that are defined by the straight lines in Fig. 4, i.e., $m_\eta \gtrsim 2m_A$, $m_A \lesssim m_h/2$ and $m_\eta \sim m_h$.

In Fig. 4 bottom-right, we show the quartic coupling λ_ϕ versus λ for the values of the coupling λ_m shown in the palette. One notes that the constraints can be escaped when the mixing coupling λ_m is small, preferably less than 0.5, and the other quartic couplings λ_ϕ and λ have values approximately greater than 10^{-3} . This result is a consequence of applying the unitarity constraints given by the last inequality in (18). Clearly, large values of both λ_ϕ and λ should be accompanied by small values of λ_m to satisfy the unitarity constraints.

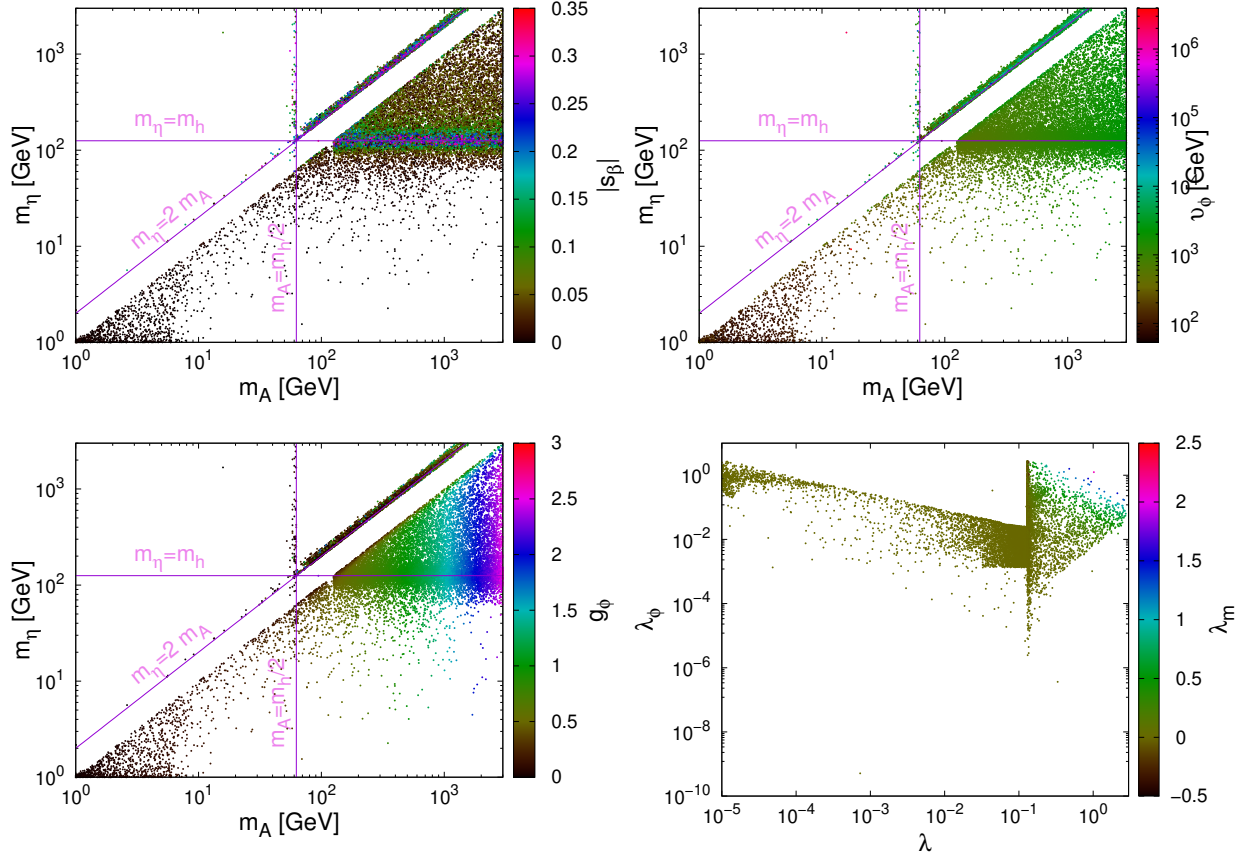


FIG. 4: The new scalar mass m_η versus the DM mass m_A , where the palette shows the scalar mixing (top-left), the new scalar vev (top-right) and the new gauge coupling (Bottom-left). Bottom-right: The quartic coupling λ_ϕ versus λ , where the coupling λ_m is shown in the palette. All the above mentioned constraints in section III are taken into account during the scan over the parameters space.

In Fig. 5, we show the signal strength (39) versus the total decay width of the new scalar (Γ_η) where the palettes show the ranges of m_β and Γ_η/m_η respectively.

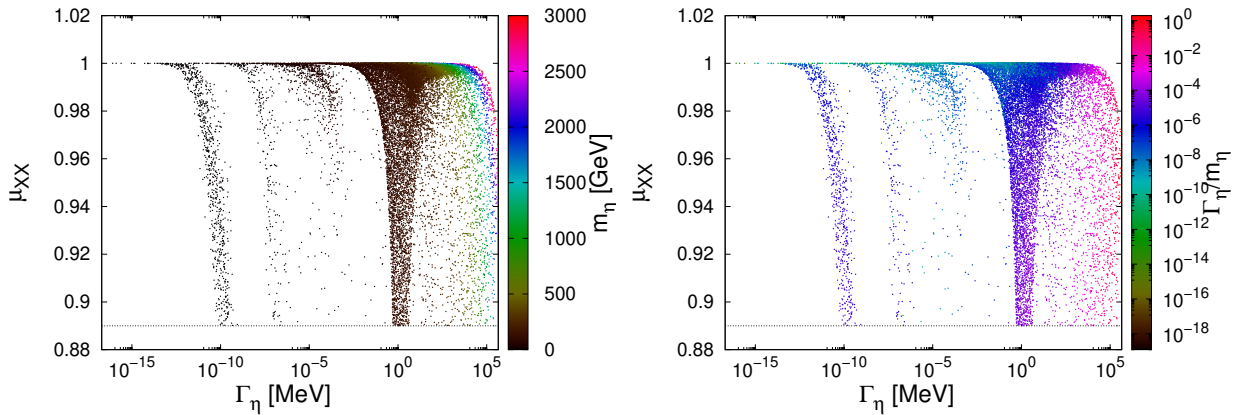


FIG. 5: The signal strength (39) versus the total decay width of the new scalar (Γ_η). The palette shows the scalar mass (m_η in GeV) mixing in left and the ratio Γ_η/m_η in right side.

From (40), the signal strength has the value c_β^2 if the Higgs decays only to SM particles, i.e., $\mathcal{B}_{BSM} = 0$, which makes small mixing values the preferred ones as shown in Fig. 5-left. From Fig. 5-right, one notices that

for $m_\eta \gtrsim 30 \text{ GeV}$, the total decay width has values $\Gamma_\eta \gtrsim 1 \text{ MeV}$, and it gets larger with large m_η values. In Fig. 6, we show the DM-nucleon direct detection cross section (24) versus the DM mass (left) and the relative contribution of each annihilation channel to the total annihilation cross section at the freeze-out temperature (right).

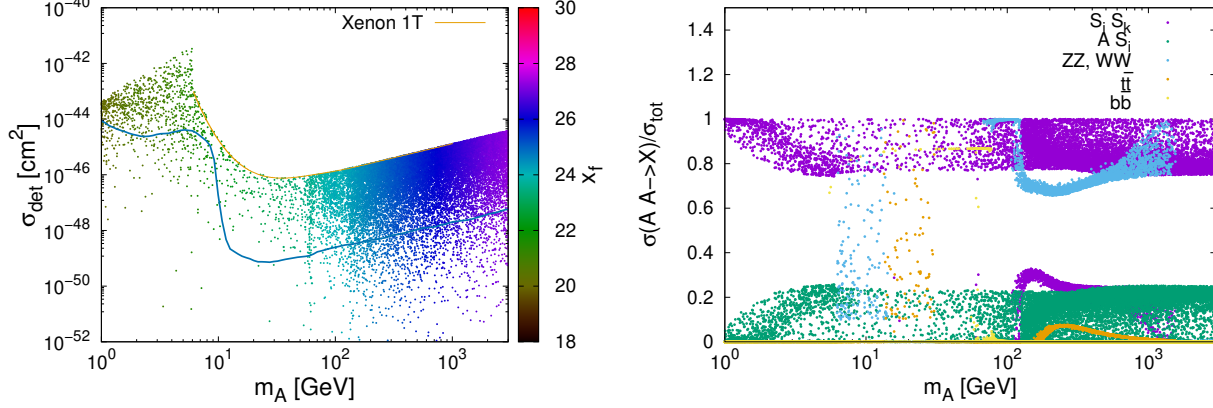


FIG. 6: Left: the DM direct detection cross section versus the DM mass, where the palette shows the freeze-out parameter $x_f = m_A/T_f$. The orange line represents the recent Xenon-1T bound [16], and the blue one represents the neutrino floor [25]. Right: the relative contributions to the thermal averaged cross section of different annihilation channels.

From Fig. 6-left, one remarks that viable dark vector DM scenario is possible at all DM masses range, and future experiments such as *Xenon-nT* [16], can probe a significant part of the parameters space. Indeed, some of the benchmark points can not be probed since they are below the neutrino floor. The freeze-out parameter $x_f = m_A/T_f$, that is shown in the palette reads typical values $x_f \sim 17 - 28$. In order to figure out which the DM annihilation channels is (are) efficient, we present in Fig. 6-right the relative contribution of each DM annihilation channel ($f\bar{f}$, WW , ZZ , hh , $\eta\eta$ and $h\eta$) to the total thermally averaged annihilation cross section at the freeze-out temperature $T_f = m_A/x_f$ versus the DM mass.

Clearly from the Fig. 6-right, one notes that the cross section tends to be dominated by the annihilation into scalar channels (hh , $\eta\eta$ and $h\eta$) which are mediated by the exchange of h , η and A_i bosons for all values of the DM mass. In addition the co-annihilation contribution (i.e., the second term in (30)) could be large as 20% of the total thermally averaged annihilation cross section. The fact that the scalar channels $\eta\eta$ is also dominant for light DM ($\mathcal{O}(\text{GeV})$) means that light DM implies light new scalar η . One has to mention also that the annihilation into gauge bosons could be efficient for DM masses around the Z mass (m_Z) and also around TeV .

In Fig. 7, we present some branching ratios of the Higgs (left), and the main branching ratios of the scalar η (right), especially $\gamma\gamma$, $A_i A_i$, hh , $t\bar{t}$, $b\bar{b}$, VV as functions of η mass.

One notices from Fig. 7-left, that the branching ratios of $h \rightarrow gg$, $h \rightarrow \gamma\gamma$ and $h \rightarrow \gamma Z$ have values close the SM ones. Concerning the invisible and undetermined branching ratios ($h \rightarrow AA$ and $h \rightarrow \eta\eta$), they can be significant within the allowed range for some of the parameters space. From Fig. 7-right, one can learn that scalar η decay can be dominated by a specific contribution for some m_η intervals. For instance, the decay into light quarks, mainly $\eta \rightarrow c\bar{c}$, dominates for the mass window $m_\eta \lesssim 8 \text{ GeV}$, while, it is dominated by $\eta \rightarrow b\bar{b}$ for $8 \text{ GeV} \lesssim m_\eta \lesssim 80 \text{ GeV}$. For the mass window $80 \text{ GeV} \lesssim m_\eta \lesssim 350 \text{ GeV}$ the decay will be dominated by $\eta \rightarrow WW, ZZ$ as well for some benchmark points with large scalar mass $m_\eta > 2.5 \text{ TeV}$. The branching ratios of $\eta \rightarrow hh$ and $\eta \rightarrow t\bar{t}$ have maximal values of 0.35 and 0.18, respectively for scalar masses larger than 400 GeV . However, the invisible channel $\eta \rightarrow AA$ could be important for few benchmark points with mass between 100 GeV and 350 GeV .

By running the RGE in (25) up to the high energy scales $\Lambda = 100 \text{ TeV}$, 10^4 TeV and $\Lambda = m_{\text{Planck}}$, we obtain the running dimensionless scalar couplings. By imposing the conditions of perturbativity, vacuum stability

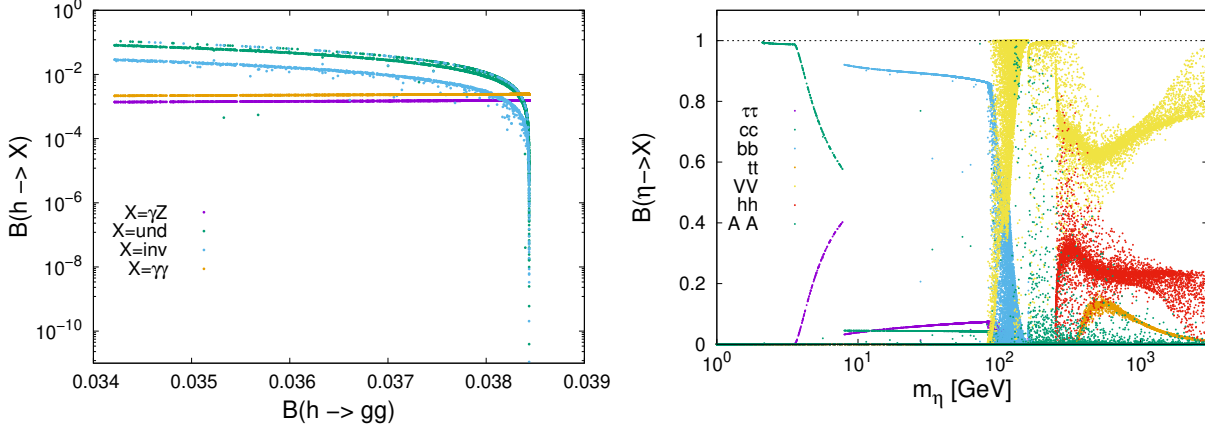


FIG. 7: Left: the Higgs branching ratios. Right: the branching ratios of the new scalar decay versus its mass.

and unitarity at these energy scales, the parameters space get reduced as shown in Fig. 8, where the plots top-left and bottom-right in Fig. 4, are obtained after after considering the above mentioned conditions.

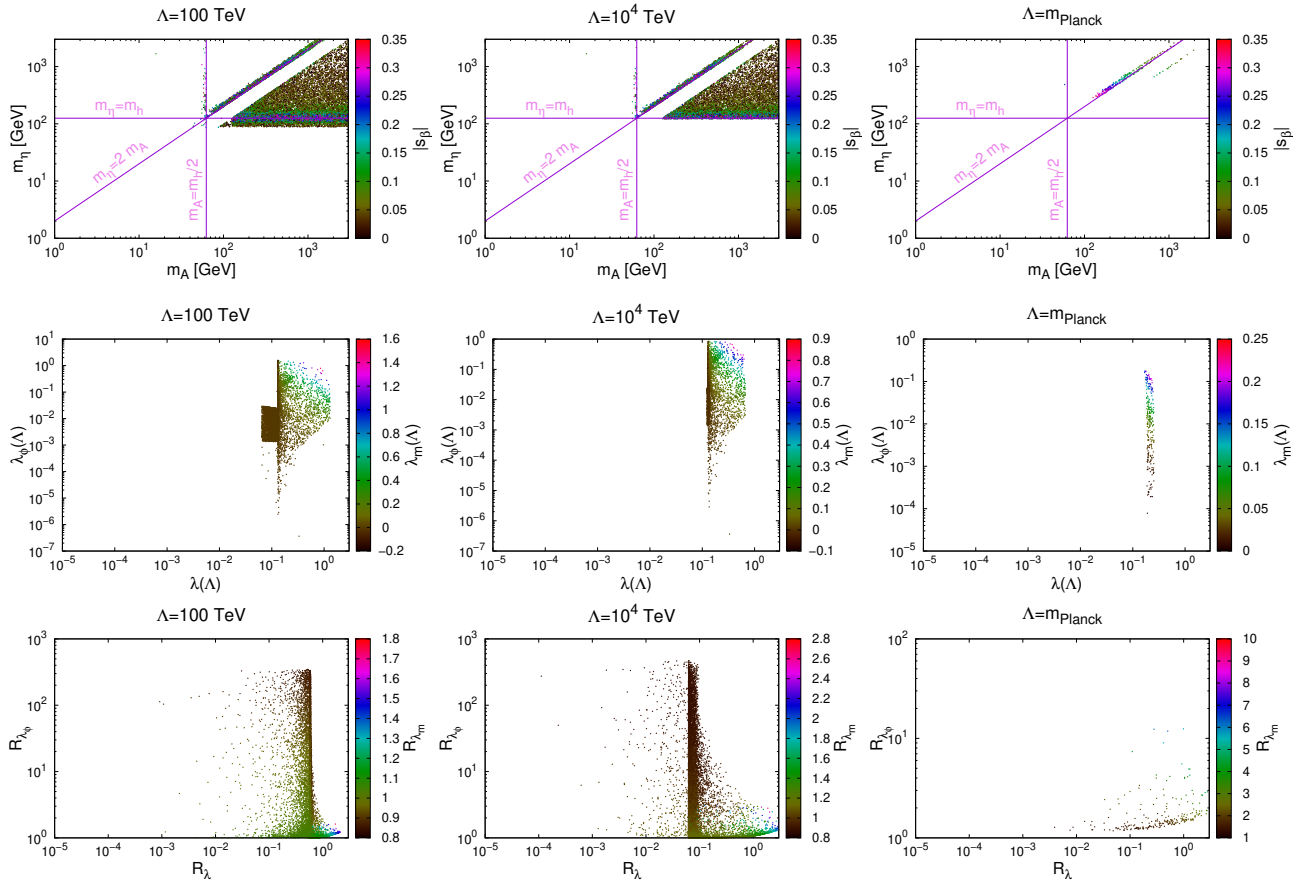


FIG. 8: Up: the updated version of Fig. 4-top-left after considering the abovementioned conditions at scales $\Lambda = 100$ TeV (left), $\Lambda = 10^4$ TeV (middle) and $\Lambda = m_{Planck}$ (right). Middle: the updated version of Fig. 4-bottom-right within similar assumptions. Bottom: we show the coupling values at the running scale, and in the bottom ones, we show their relative enhancement $R_{\lambda_i}(\Lambda) = \lambda_i(\Lambda)/\lambda_i(m_Z)$.

At higher scales, only benchmarks with non-suppressed λ fulfills the above-mentioned conditions. In addition, only benchmarks points with positive λ_m are favored. The enhancement in λ_ϕ could be two or-

ders of magnitude larger, which allows benchmark points with small λ_ϕ values. For instance, for 20k benchmark points shown in Fig. 4, the conditions of perturbativity, vacuum stability and unitarity at the scales $\Lambda = 100 \text{ TeV}$, 10^4 TeV and $\Lambda = m_{\text{Planck}}$, are fulfilled only for 16700, 11900 and 260, respectively.

B. Triple Higgs Coupling

In the SM, electroweak symmetry breaking relies on the parameters in the Higgs scalar potential, namely on the choice $\mu^2 < 0$ and $\lambda > 0$. Hence, the partial experimental reconstruction of the Higgs scalar potential through measuring the triple Higgs coupling, λ_{hhh} , turns to be crucial to verify that the symmetry breaking is due to a SM-like Higgs sector [26]. Not only this, but it can also shed light on new physics [27] knowing that in many extensions of the SM, λ_{hhh} can be modified by Higgs mixing effects or higher order corrections induced by new particles as we will show below. Consequently, the measurement of λ_{hhh} is a crucial task in the LHC, although being challenging [26, 28], and future collider experiments.

Indirect probe of the triple Higgs coupling can be carried out through investigating the loop effects in some observables such as the single Higgs production [29–31], and the electroweak precision observables [32]. Using the 80 fb^{-1} of LHC Run-2 data, and upon the assumption that new physics can affect only λ_{hhh} , ATLAS collaboration set recently the bound $-1.5 < \lambda_{hhh}/\lambda_{hhh}^{SM} < 6.7$ at 95% CL [33]. It should be noted that, direct measurement of the triple Higgs coupling at the LHC is possible and can be achieved through the di-Higgs production. This production is dominated by the gluon-gluon fusion process. In the SM, the production has two main contributions originating from the triangle diagram induced by the triple Higgs coupling, and from the box diagram with the top quark running in the loop. As noted in [34], the two amplitudes, corresponding to the two contributions, interfere destructively. Consequently, at next-to-next-to-next-to-leading order (N³LO) and after including finite top quark mass effects, the estimated cross section at 14 TeV LHC turn to be small and equal to 38.65 fb [34].

The analysis of the potential of measuring the di-Higgs production in the decay channels $b\bar{b}b\bar{b}$, $b\bar{b}\tau^+\tau^-$, $b\bar{b}WW^*$, $\gamma\gamma b\bar{b}$, $\gamma\gamma WW^*$ and WW^*WW^* , has been carried out in Refs. [26, 28, 35–49]. At 13 TeV LHC with the luminosity of 36.1 fb^{-1} , the combination of the six analyses results in the constraint $-5 < \lambda_{hhh}/\lambda_{hhh}^{SM} < 12$ at 95% CL [50]. It is expected that, the sensitivity will be highly improved at the high-luminosity upgrade of the LHC (HL-LHC) [23] and future hadron colliders [51]. For instances, the future circular hadron collider, FCC- hh , with a center-of-mass energy of 100 TeV and an integrated luminosity of 30 ab^{-1} of data will allow reaching a 5% accuracy (at 68% CL) on the measurement of the triple Higgs coupling [23, 49, 52].

The initial phase of the International Linear Collider (ILC) with a center-of-mass energy of $\sqrt{s} = 250 \text{ GeV}$ cannot directly probe λ_{hhh} via di-Higgs production [53]. However, this is not the case regarding single-Higgs production where an analysis using 2 ab^{-1} of data can allow a measurement to 49% accuracy, at 68% CL [54]. Higher precision of 27% or 10%, at 68% CL, could possibly be reached using the data from ILC extensions to 500 GeV (4 ab^{-1}) or 1 TeV (8 ab^{-1}) respectively [55, 56]. Moreover, at the same value of the confidence level, a more higher accuracy of $0.93 < \lambda_{hhh}/\lambda_{hhh}^{SM} < 1.11$ is possible to be reached using the combination of 1 ab^{-1} of data at 380 GeV , 2.5 ab^{-1} at 1.5 TeV , and 5 ab^{-1} at 3 TeV expected to be collected in the CLIC project [56–59].

In our model, the triple Higgs coupling λ_{hhh} gets modified due to the mixing with the scalar η , and in addition, it receives new one-loop contributions by the scalar η and the new gauge bosons A_i . Taking these contributions into account, we can parameterize λ_{hhh} as

$$\lambda_{hhh} = \lambda_{hhh}^{SM}(1 + \Delta_{hhh}), \quad (42)$$

where the one-loop triple Higgs coupling in the SM is given by [60, 61]

$$\lambda_{hhh}^{SM} \simeq \frac{3m_h^2}{v} \left[1 - \frac{m_t^4}{\pi^2 v^2 m_h^2} \right]. \quad (43)$$

According to the ILC physics group, the triple Higgs coupling can be measured at $\sqrt{s} = 500 \text{ GeV}$ within the integrated luminosity $\mathcal{L} = 500 \text{ fb}^{-1}$ with an accuracy less or equal to 20% [55]. This implies that for

the parameters space where $m_\eta \gg m_h^2$, our model can be tested at future linear colliders. Here, we estimate the parameter Δ_{hhh} following [62], where the Higgs trilinear self-coupling can be considered as the third derivative of the Higgs one-loop effective potential

$$\lambda_{hhh} = \frac{\partial^3 V_{eff}}{\partial h^3}, \quad (44)$$

where, the zero temperature one-loop effective potential $V_{eff}(h', \eta')$ is described in Appendix A. Therefore, one writes

$$\lambda_{hhh} = c_\beta^3 \frac{\partial^3 V_{eff}}{\partial h'^3} - 3c_\beta^2 s_\beta \frac{\partial^3 V_{eff}}{\partial \eta' \partial h'^2} + 3c_\beta s_\beta^2 \frac{\partial^3 V_{eff}}{\partial \eta'^2 \partial h'} - s_\beta^3 \frac{\partial^3 V_{eff}}{\partial \eta'^3} \Big|_{h'=\eta'=0}. \quad (45)$$

At tree-level, these scalar triple couplings correspond to the ρ_h parameter given in (15). For the benchmark points used previously, we show the Higgs triple coupling relative enhancement in Fig. 9.

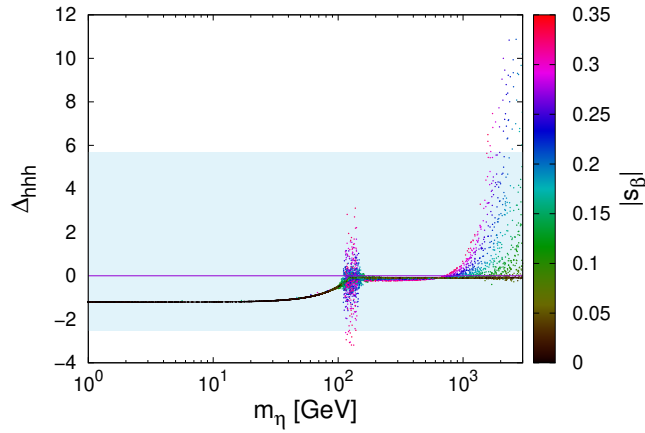


FIG. 9: The triple Higgs relative enhancement Δ_{hhh} versus the new scalar mass, where the palette shows the scalar mixing. The skyblue band represents the allowed values of Δ_{hhh} by the recent ATLAS measurements [33].

The effect of these extra contributions can be either constructive or destructive according to the η mass range. For instance, from Fig. 11, one notices that for scalar mass $m_\eta < m_h$ the coupling (44) is almost suppressed. While for the degenerate case $m_\eta \sim m_h$, we could have either enhancement or suppression. For η mass larger than 1.2 TeV, some benchmark points are already suppressed by the ATLAS recent measurements [33].

C. The Di-Higgs Production

The di-Higgs production is not only interesting as its measurement allows to determine the trilinear Higgs couplings but also to describe the EWSB, i.e., it occurs via one Higgs or more. The triple Higgs coupling can be measured directly in di-Higgs boson production at ILC through double Higgs-strahlung off W or Z bosons [63–67], WW or ZZ fusion [65–71], also through gluon-gluon fusion in pp collisions at the LHC [72–74]. The Higgs pair production processes in this model can be achieved three via Feynman diagrams as shown in Fig. 10. Indeed, there are two triangle diagrams mediated by the Higgs field h and the new singlet scalar field η instead of one diagram in the SM.

In the SM, the di-Higgs production cross section has three contributions

$$\sigma^{SM}(hh) = \sigma_\square + \sigma_\Delta + \sigma_{\Delta\square}, \quad (46)$$

² In this model, the relevant process that probes the triple Higgs coupling at the ILC ($e^+e^- \rightarrow Zh h @ 500 \text{ GeV}$), occurs via another Feynman diagram mediated by the new scalar η . Therefore, if $m_\eta \gtrsim 400 \text{ GeV} \gg m_h$ this new diagram is subleading and therefore the triple Higgs coupling can be probed similarly to the case of single Higgs models.

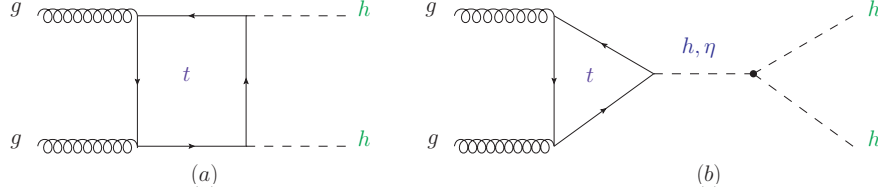


FIG. 10: Feynman diagrams that contribute to the di-Higgs production via gluon fusion. The left (right) diagram is referred to be the box (triangle) in the literature.

which correspond to the box ($\sigma_{\square} = 70.1 fb$), triangle ($\sigma_{\Delta} = 9.66 fb$); and interference ($\sigma_{\Delta\square} = -49.9 fb$), respectively [75]. In this model, the di-Higgs production cross section can be written as

$$\sigma(hh) = \xi_1 \sigma_{\square} + \xi_2 \sigma_{\Delta} + \xi_3 \sigma_{\Delta\square}, \quad (47)$$

where the SM corresponds to $s_{\beta} = 0$, i.e., $\xi_1 = \xi_2 = \xi_3 = 1$. The coefficients ξ_i in our model are modified with respect to the SM as

$$\xi_1 = c_{\beta}^4, \quad \xi_2 = \left(c_{\beta} \frac{\rho_h}{\lambda_{hhh}^{SM}} + s_{\beta} \frac{\rho_2}{\lambda_{hhh}^{SM}} \frac{s - m_h^2}{s - m_{\eta}^2} \right)^2, \quad \xi_3 = c_{\beta}^2 \left(c_{\beta} \frac{\rho_h}{\lambda_{hhh}^{SM}} + s_{\beta} \frac{\rho_2}{\lambda_{hhh}^{SM}} \frac{s - m_h^2}{s - m_{\eta}^2} \right), \quad (48)$$

with ρ_h and ρ_2 are defined in (15), λ_{hhh}^{SM} the Higgs triple coupling in the SM is given in (43); and \sqrt{s} is the CM collision energy, which we will consider to be $\sqrt{s} = 14 TeV$. In Fig. 11-left, we show the di-Higgs production cross section (47) at LHC14 scaled by its SM value versus the new scalar mass m_{η} and the scalar mixing (in the palette), and in Fig. 11-right, we present the parameters ξ 's (48) for the benchmark points used previously.

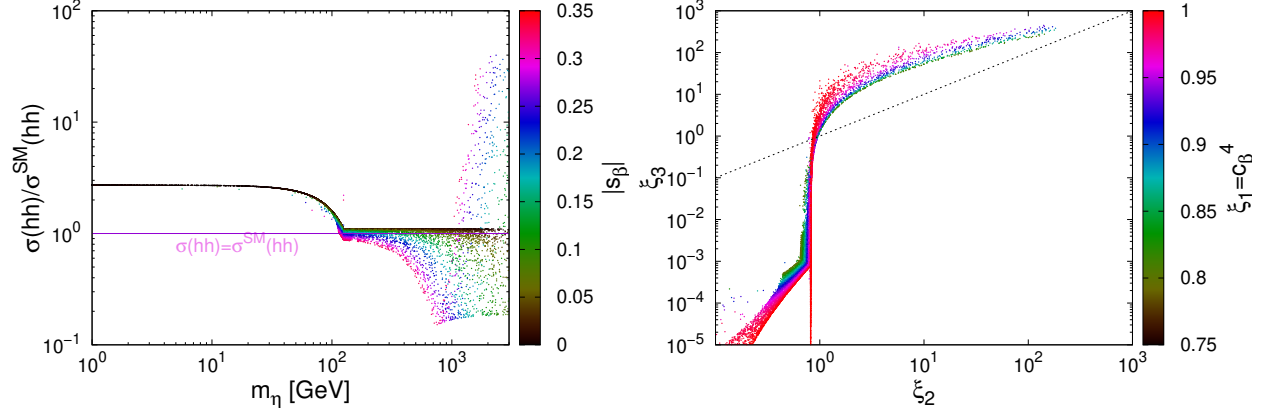


FIG. 11: Left: the di-Higgs production cross section at 14 TeV, scaled by the SM value, where the palette shows the scalar mixing. Right: the parameters ξ 's (48) for the benchmark points used previously. The dashed line represent $\xi_2 = \xi_3$, above which the destructive interference contribution in (47) is larger, and hence the total cross section is reduced.

Clearly for lighter new scalar $m_{\eta} < m_h$ the di-Higgs cross section masses is larger than the SM values by around 180 %, while, for heavier η scalar $m_{\eta} > m_h$, it lies between -92 % and 3000 %. Indeed, not all of the benchmark points would be in agreement with current data. In order to understand these results, Fig. 11-right shows the relation between the parameters ξ_2 and ξ_3 , where ξ_1 is shown in the palette. Since the interference term in (47) is negative, then the benchmark points above the straight line $\xi_2 = \xi_3$ in Fig. 11-right correspond to larger cross section values. For lighter η scalar $m_{\eta} < m_h/2$, where the undetermined Higgs decay channel $h \rightarrow \eta\eta$ is open, more negative searches can be used to constrain the parameters space, especially via the signatures $h \rightarrow \eta\eta \rightarrow bb\mu\mu$ [76], $h \rightarrow \eta\eta \rightarrow 4b$ [77]; and $h \rightarrow \eta\eta \rightarrow \gamma\gamma jj$ [78]. This analysis is postponed for a future work [79].

VI. CONCLUSION

In this work, we have considered an extension of the SM by enlarging the SM gauge symmetry by a non-abelian gauge group $SU(2)_{HS}$. In this case, the scalar sector of the model contains an extra new Higgs doublet that is required to spontaneously break the $SU(2)_{HS}$ gauge symmetry. The mixing of the extra doublet with the SM Higgs results, in the mass eigenstates basis, in two scalars denoted by h and η . In our analysis, we identified h as the SM neutral Higgs-like boson and adopted its mass to be 125 GeV . An important feature of the model is that the new gauge bosons, A_i^μ with $i=1,2,3$, associated with the group $SU(2)_{HS}$ are exactly degenerate in mass and can serve as vector DM candidates that interact with the SM through the Higgs portal.

To investigate such a possibility for DM candidate, we first considered all relevant constraints on the model, which include both theoretical and experimental ones, such as perturbative unitarity, vacuum stability, perturbativity, experimental bound on the DM direct detection, the observed DM relic density, the constraints from the Higgs decay where the invisible or/and undetermined branching ratio where the Higgs total decay width must respect the existing experimental constraints. As a result, we showed that it is possible to have viable parameters space in which the masses of the DM candidates lies from few GeV to the TeV scale, which is still within the reach of high energy collider experiments. Regarding the limits from direct detection DM experiments, it is easily acomodated in this model for most of the values of DM and new scalar masses. In addition, the observed relic density values can be achieved by many anihilation channels according to the DM mass, and on top of that, the co-anihilation ($A_i A_j \rightarrow h A_k$) effect could be important as it may reach 25 % of the total thermally averaged anihilation cross section.

In our work, we considered the conditions of perturbativity, vacuum stability and perturbative unitarity, but these conditions may not be fulfilled at higher scales. By running the quartic scalar and gauge couplings at higher scale Λ using the RGE (25), we found that 16.5 %, 40 % and 98.7 % of the benchmark points will be ruled out due these conditions at scale values $\Lambda = 100 \text{ TeV}$, 10^4 TeV , m_{Planck} , respectively.

In the decoupling limit $m_\eta \gg m_h$, as in many extensions of the SM, the Higgs mixing effects and the presence of new fields coupled to the Higgs doublet induces significant corrections to the SM prediction of the triple Higgs self-couplings $\lambda_{hhh} = (1 + \Delta_{hhh})\lambda_{hhh}^{SM}$. We have found that, up to one-loop level, the effect of the new scalar η and the vector DM A_i leads to a relative enhancement (Δ_{hhh}) that lies between -250 % and +1200 %. Indeed, part of these benchmark points are already excluded by the recent measurements by ATLAS [33]. However, in the case $m_\eta < m_h$, the cross the di-Higgs gets enhanced by around 180 %, which makes the signatures $h \rightarrow \eta\eta \rightarrow bb\mu\mu$, $h \rightarrow \eta\eta \rightarrow 4b$ and $h \rightarrow \eta\eta \rightarrow \gamma\gamma jj$ very useful to put more constraints on the model free parameters.

Appendix A: The One-Loop Effective Potential

The zero temperature one-loop effective potential can be given in the \overline{DR} scheme by

$$V_{eff}(h', \eta') = V^0(h', \eta') + \frac{1}{64\pi^2} \sum_i n_i m_i^4(h', \eta') \left(\log \left(\frac{m_i^2(h', \eta')}{\Lambda^2} \right) - \frac{3}{2} \right),$$

where, $V^0(h', \eta')$ is the tree-level potential, n_i is the number of internal degrees of freedom of the i th particle ($n_h = n_\eta = 1$, $n_Z = 3$, $n_W = 6$, $n_t = -12$ and $n_{A_i} = 9$). Here, $m_i^2(h', \eta')$ are the field-dependent squared masses; and Λ is the renormalization scale, which we will choose to be the Higgs mass $\Lambda = 125.18 \text{ GeV}$.

The field-dependent squared masses $m_i(h', \eta')$ of all the contributing particles, so we have the field-dependent masses of the Goldstone bosons χ and $\tilde{\zeta}$

$$m_\chi^2 = \mu^2 + \lambda h'^2 + \frac{\lambda_m}{2} \eta'^2, \quad m_{\tilde{\zeta}}^2 = \mu_\phi^2 + \lambda_\phi \eta'^2 + \frac{\lambda_m}{2} h'^2. \quad (\text{A1})$$

The field-dependent masses of the electroweak gauge bosons and top quark are given in the symmetric phase (i.e., for $\langle h \rangle = \langle \phi \rangle = 0$) by

$$m_t^2 = \frac{y_t^2}{2} h'^2, m_W^2 = \frac{g_2^2}{4} h'^2, m_{W^3}^2 = \frac{g_2^2}{4} h'^2, m_{W^3-B}^2 = \frac{g_1^2}{4} h'^2, m_B^2 = \frac{g_1^2}{4} h'^2, m_A^2 = \frac{g_\phi^2}{4} \eta'^2, \quad (\text{A2})$$

where the diagonalization of the $\{W^3 - B\}$ matrix gives $m_\gamma = 0$ and $m_Z^2 = \frac{(g_1^2 + g_2^2)}{4} h'^2$. Here, y_t denotes the top-quark Yukawa coupling, and g_1 , g_2 and g_ϕ are the gauge couplings of $U(1)_Y$, $SU(2)_L$ and $SU(2)_{HS}$, respectively.

For the field-dependent masses of h and η can be obtained as the eigensvalues of the squared mass matrice in the basis $\{h', \eta'\}$, which is given by

$$M^2 = \begin{pmatrix} A & C \\ C & B \end{pmatrix}, \quad (\text{A3})$$

with $A = \mu^2 + 3\lambda h'^2 + \frac{\lambda_m}{2} \eta'^2$, $B = \mu_\phi^2 + 3\lambda_\phi \eta'^2 + \frac{\lambda_m}{2} h'^2$, $C = \lambda_m h' \eta'$. Then, the field dependant eigenmasses are given by $m_{h,\eta}^2(h', \eta') = \frac{1}{2} \left(A + B \mp \sqrt{(A - B)^2 + C^2} \right)$.

Appendix B: The Cross Section for $hh, \eta\eta, h\eta, Ah$ & $A\eta$

Here, we give the formulas of the parameters used in the cross section of the final states $hh, \eta\eta, h\eta, Ah$ & $A\eta$ given in (34), (36) and (35). We denote by H either h or η , so the parameters are given by

$$\begin{aligned} A &= \frac{2m_H^2 - s}{2m_A^2}, B = \frac{s}{2m_A^2} \sqrt{\left(1 - \frac{4m_H^2}{s}\right) \left(1 - \frac{4m_A^2}{s}\right)}, Q_0 = \frac{\sqrt{1 - \frac{4m_H^2}{s}}}{16\pi}, \\ Q_1 &= \frac{2q^4}{9v_\phi^4 m_A^4} (48m_A^8 - 32m_A^6 m_H^2 + 24m_A^4 m_H^4 - 16m_A^4 m_H^2 s + 4m_A^4 s^2 - 8m_A^2 m_H^6 + 4m_A^2 m_H^4 s + m_H^8), \\ Q_2 &= \frac{4q^4}{9v_\phi^4 m_A^2 (s - 2m_H^2)} (-48m_A^8 + 32m_A^6 m_H^2 - 8m_A^4 m_H^4 + 4m_A^4 s^2 - 8m_A^2 m_H^6 + 4m_A^2 m_H^2 s^2 - 2m_A^2 s^3 \\ &\quad + 3m_H^8 - m_H^4 s^2) + \frac{4q^2 \Re(R)}{9v_\phi^4 m_A^2 (s - 2m_H^2)} (-48m_A^6 m_H^2 + 24m_A^6 s + 16m_A^4 m_H^4 - 4m_A^4 s^2 - 4m_A^2 m_H^6 \\ &\quad + 10m_A^2 m_H^4 s - 8m_A^2 m_H^2 s^2 + 2m_A^2 s^3 - 2m_H^6 s + m_H^4 s^2), \\ Q_3 &= \frac{4q^4}{9v_\phi^4} (-4m_A^4 + 4m_A^2 m_H^2 - 6m_A^2 s + m_H^4 + 2m_H^2 s) + \frac{8q^2 \Re(R)}{9v_\phi^4} (-4m_A^2 m_H^2 + 4m_A^2 s - m_H^2 s) \\ &\quad + \frac{|R|^2}{9v_\phi^4} (12m_A^4 - 4m_A^2 s + s^2), \\ Q_4 &= \frac{4m_A^2 q^4}{9v_\phi^4 (2m_H^2 - s)} (8m_A^4 - 8m_A^2 m_H^2 + 8m_A^2 s + 2m_H^4 - 4m_H^2 + s^2) + \frac{4m_A^2 q^2 \Re(R)}{9v_\phi^4 (2m_H^2 - s)} (4m_A^2 m_H^2 \\ &\quad - 2m_A^2 s + 2m_H^2 s - s^2), Q_5 = -\frac{2q^4 m_A^4}{3v_\phi^4}, Q_6 = \frac{4q^4 m_A^6}{9v_\phi^4 (2m_H^2 - s)}. \end{aligned} \quad (\text{B1})$$

with $\{q, R\} = \left\{ s\beta, \frac{c_{\beta\rho_2} v_\phi}{s - m_\eta^2 + im_\eta \Gamma_\eta} - \frac{s\beta\rho_h v_\phi}{s - m_h^2 + im_h \Gamma_h} + s_\beta^2 \right\}$ for h ; and $\{q, R\} = \left\{ -c_\beta, \frac{s\beta\rho_\eta v_\phi}{s - m_\eta^2 + im_\eta \Gamma_\eta} + \frac{c_{\beta\rho_1} v_\phi}{s - m_h^2 + im_h \Gamma_h} + c_\beta^2 \right\}$ for η , where Γ_h (Γ_η) is the total decay width of the Higgs (scalar η).

For the final state $h\eta$, the parameters are given by

$$\begin{aligned}
A &= \frac{m_h^2 + m_\eta^2 - s}{2m_A^2}, \quad B = \frac{1}{2m_A^2} \sqrt{1 - \frac{4m_A^2}{s}} \sqrt{(s - m_h^2 - m_\eta^2)^2 - 4m_h^2 m_\eta^2}, \\
Q_0 &= \frac{\sqrt{(s - m_h^2 - m_\eta^2)^2 - 4m_h^2 m_\eta^2}}{16\pi s}, \quad R = -\frac{s_\beta \rho_2 v_\phi}{s - m_h^2 + im_h \Gamma_h} + \frac{c_\beta \rho_1 v_\phi}{s - m_\eta^2 + im_\eta \Gamma_\eta} - c_\beta s_\beta, \\
Q_1 &= \frac{s_{2\beta}^2}{36m_A^4 v_\phi^4} (48m_A^8 - 16m_A^6 m_\eta^2 - 16m_A^6 m_h^2 + 8m_A^4 m_\eta^4 + 8m_A^4 m_\eta^2 m_h^2 - 8m_A^4 m_\eta^2 s + 8m_A^4 m_h^4 - 8m_A^4 m_h^2 s \\
&\quad + 4m_A^4 s^2 - 4m_A^2 m_\eta^4 m_h^2 - 4m_A^2 m_\eta^2 m_h^4 + 4m_A^2 m_\eta^2 m_h^2 s + m_\eta^4 m_h^4), \\
Q_2 &= \frac{s_{2\beta}^2}{18m_A^2 v_\phi^4} (-4m_A^4 m_\eta^2 - 4m_A^4 m_h^2 + 8m_A^4 s + 8m_A^2 m_\eta^2 m_h^2 - 2m_A^2 m_\eta^2 s - 2m_A^2 m_h^2 s - m_\eta^4 m_h^2 - m_\eta^2 m_h^4) \\
&\quad + \frac{\Re(R) s_{2\beta}}{9m_A^2 v_\phi^4} (-24m_A^6 + 4m_A^4 m_\eta^2 + 4m_A^4 m_h^2 + 4m_A^4 s - 2m_A^2 m_\eta^4 + 2m_A^2 m_\eta^2 m_h^2 + 2m_A^2 m_\eta^2 s - 2m_A^2 m_h^4 \\
&\quad + 2m_A^2 m_h^2 s - 2m_A^2 s^2 - m_\eta^2 m_h^2 s), \\
Q_3 &= \frac{|R|^2}{9v_\phi^4} (12m_A^4 - 4m_A^2 s + s^2) + \frac{s_{2\beta} \Re(R)}{9v_\phi^4} (2m_A^2 m_\eta^2 + 2m_A^2 m_h^2 - 4m_A^2 s + m_\eta^2 s + m_h^2 s) \\
&\quad + \frac{s_{2\beta}^2}{36v_\phi^4} (8m_A^4 - 4m_A^2 m_\eta^2 - 4m_A^2 m_h^2 + 4m_A^2 s + 4m_\eta^2 m_h^2 + m_\eta^4 + m_h^4), \\
Q_4 &= -\frac{s_{2\beta} \Re(R) m_A^2}{9v_\phi^4} (2m_A^2 + s) - \frac{s_{2\beta}^2 m_A^2}{18v_\phi^4} (m_\eta^2 + m_h^2), \quad Q_5 = \frac{s_{2\beta}^2 m_A^4}{36 v_\phi^4}, \quad Q_6 = 0.
\end{aligned} \tag{B2}$$

For the final states Ah and $A\eta$, the parameters are given by

$$\begin{aligned}
A &= \frac{m_A^2 + m_H^2 - s}{2m_A^2}, \quad B = \frac{1}{2m_A^2} \sqrt{1 - \frac{4m_A^2}{s}} \sqrt{(s - m_H^2 - m_A^2)^2 - 4m_H^2 m_A^2}, \\
Q_0 &= \frac{\sqrt{(s - m_H^2 - m_A^2)^2 - 4m_H^2 m_A^2}}{16\pi s}, \\
Q_1 &= -\frac{q^2}{36m_A^4 v_\phi^4} (20m_A^8 + 588m_A^6 m_H^2 + 256m_A^6 s - 461m_A^4 m_H^4 - 352m_A^4 m_H^2 s - 96m_A^4 s^2 \\
&\quad + 72m_A^2 m_H^6 + 108m_A^2 m_H^4 s + 128m_A^2 m_H^2 s^2 - 36m_H^4 s^2), \\
Q_2 &= -\frac{q^2}{18m_A^2 v_\phi^4 (s - m_A^2)} (336m_A^8 - 165m_A^6 m_H^2 - 264m_A^6 s - 37m_A^4 m_H^4 + 241m_A^4 m_H^2 s \\
&\quad + 128m_A^4 s^2 - 21m_A^2 m_H^4 s - 88m_A^2 m_H^2 s^2 - 32m_A^2 s^3 - 18m_H^4 s^2 + 36m_H^2 s^3), \\
Q_3 &= \frac{q^2}{36v_\phi^4 (s - m_A^2)^2} (-591m_A^8 + 480m_A^6 m_H^2 - 302m_A^6 s + m_A^4 m_H^4 - 416m_A^4 m_H^2 s \\
&\quad + 189m_A^4 s^2 + 6m_A^2 m_H^4 s + 104m_A^2 m_H^2 s^2 - 100m_A^2 s^3 + 9m_H^4 s^2 - 72m_H^2 s^3 + 36s^4), \\
Q_4 &= \frac{q^2 m_A^2}{18v_\phi^4 (s - m_A^2)^2} (-153m_A^6 - 69m_A^4 m_H^2 + 164m_A^4 s - 2m_A^2 m_H^2 s - 29m_A^2 s^2 - 9m_H^2 s^2 + 18s^3), \\
Q_5 &= \frac{q^2 m_A^4}{36v_\phi^4 (s - m_A^2)^2} (153m_A^4 - 2m_A^2 s + 9s^2), \quad Q_6 = 0,
\end{aligned} \tag{B3}$$

with $\{m_H, q^2\} = \{m_h, s_\beta\}, \{m_\eta, -c_\beta\}$ for the final states Ah and $A\eta$, respectively.

-
- [1] F. Zwicky, *Helv. Phys. Acta* **6**, 110 (1933) [Gen. Rel. Grav. **41**, 207 (2009)]. E. Corbelli and P. Salucci, *Mon. Not. Roy. Astron. Soc.* **311**, 441 (2000) [arXiv:astro-ph/9909252 [astro-ph]]. D. P. Roy, [arXiv:physics/0007025 [physics]]. I
- [2] N. Aghanim *et al.* [Planck], *Astron. Astrophys.* **641**, A6 (2020) [arXiv:1807.06209 [astro-ph.CO]]. I
- [3] For example: N. G. Deshpande and E. Ma, *Phys. Rev. D* **18**(1978), 2574 S. Hannestad, A. Mirizzi, G. G. Raffelt and Y. Y. Y. Wong, *JCAP* **04** (2008), 019 [arXiv:0803.1585 [astro-ph]]. T. Hambye and M. H. G. Tytgat, *Phys. Lett. B* **659**, 651 (2008) [arXiv:0707.0633 [hep-ph]]. A. Ahriche and S. Nasri, *Phys. Rev. D* **85** (2012), 093007 [arXiv:1201.4614 [hep-ph]]. C. Gross, O. Lebedev and T. Toma, *Phys. Rev. Lett.* **119**, no.19, 191801 (2017) [arXiv:1708.02253 [hep-ph]]. Y. Abe, T. Toma and K. Tsumura, *JHEP* **05**(2020), 057 [arXiv:2001.03954 [hep-ph]]. N. Okada, D. Raut and Q. Shafi, [arXiv:2001.05910 [hep-ph]]. A. Ahmed, S. Najjari and C. B. Verhaaren, *JHEP* **06**(2020), 007 [arXiv:2003.08947 [hep-ph]]. J. McDonald, *Phys. Rev. D* **50**(1994), 3637 [arXiv:hep-ph/0702143 [hep-ph]]. J. McDonald, *Phys. Rev. Lett.* **88**, 091304 (2002) [arXiv:hep-ph/0106249 [hep-ph]]. C. P. Burgess, M. Pospelov and T. ter Veldhuis, *Nucl. Phys. B* **619**, 709 (2001) [arXiv:hep-ph/0011335 [hep-ph]]. C. Boehm and P. Fayet, *Nucl. Phys. B* **683**, 219 (2004) [arXiv:hep-ph/0305261 [hep-ph]]. C. Boehm, Y. Farzan, T. Hambye, S. Palomares-Ruiz and S. Pascoli, *Phys. Rev. D* **77** (2008), 043516 [arXiv:hep-ph/0612228 [hep-ph]]. V. Barger, P. Langacker, M. McCaskey, M. J. Ramsey-Musolf and G. Shaughnessy, *Phys. Rev. D* **77** (2008), 035005 [arXiv:0706.4311 [hep-ph]]. S. Andreas, T. Hambye and M. H. G. Tytgat, *JCAP* **10** (2008), 034 [arXiv:0808.0255 [hep-ph]]. I
- [4] For example: P. Nath and R. L. Arnowitt, [arXiv:hep-ph/9610460 [hep-ph]]. N. Baouche and A. Ahriche, *Phys. Rev. D* **96** (2017), 055029 [arXiv:1707.05263 [hep-ph]]. L. Covi, L. Roszkowski, R. Ruiz de Austri and M. Small, *JHEP* **06**(2004), 003 [arXiv:hep-ph/0402240 [hep-ph]]. M. Pospelov, A. Ritz and M. B. Voloshin, *Phys. Lett. B* **662**, 53 (2008) [arXiv:0711.4866 [hep-ph]]. G. Belanger, A. Pukhov and G. Servant, *JCAP* **01**(2008), 009 [arXiv:0706.0526 [hep-ph]]. L. Covi, M. Grefe, A. Ibarra and D. Tran, *JCAP* **01**(2009), 029 [arXiv:0809.5030 [hep-ph]]. S. Ipek, D. McKeen and A. E. Nelson, *Phys. Rev. D* **90**(2014), no.5, 055021 [arXiv:1404.3716 [hep-ph]]. K. Ghorbani, *JCAP* **01**(2015), 015 [arXiv:1408.4929 [hep-ph]]. A. Ahriche and S. Nasri, *JCAP* **07** (2013), 035 [arXiv:1304.2055 [hep-ph]]. A. Ahriche, C. S. Chen, K. L. McDonald and S. Nasri, *Phys. Rev. D* **90** (2014), 015024 [arXiv:1404.2696 [hep-ph]]. A. Ahriche, K. L. McDonald and S. Nasri, *JHEP* **10** (2014), 167 [arXiv:1404.5917 [hep-ph]]. A. Ahriche, K. L. McDonald, S. Nasri and T. Toma, *Phys. Lett. B* **746** (2015), 430-435 [arXiv:1504.05755 [hep-ph]]. A. Ahriche, K. L. McDonald and S. Nasri, *JHEP* **02** (2016), 038 [arXiv:1508.02607 [hep-ph]]. A. Ahriche, K. L. McDonald, S. Nasri and I. Picek, *Phys. Lett. B* **757** (2016), 399-404 [arXiv:1603.01247 [hep-ph]]. A. Ahriche, A. Manning, K. L. McDonald and S. Nasri, *Phys. Rev. D* **94** (2016) no.5, 053005 [arXiv:1604.05995 [hep-ph]]. A. Ahriche, A. Jueid and S. Nasri, *Phys. Rev. D* **97** (2018) no.9, 095012 [arXiv:1710.03824 [hep-ph]]. A. Ahriche, A. Arhrib, A. Jueid, S. Nasri and A. de La Puente, *Phys. Rev. D* **101** (2020) no.3, 035038 [arXiv:1811.00490 [hep-ph]]. A. Ahriche, A. Jueid and S. Nasri, *Phys. Lett. B* **814** (2021), 136077 [arXiv:2007.05845 [hep-ph]]. S. Baek, P. Ko and J. Li, *Phys. Rev. D* **95**(2017), no.7, 075011 [arXiv:1701.04131 [hep-ph]]. I
- [5] For example: H. C. Cheng, J. L. Feng and K. T. Matchev, *Phys. Rev. Lett.* **89**, 211301 (2002) [arXiv:hep-ph/0207125 [hep-ph]]. D. Hooper and G. D. Kribs, *Phys. Rev. D* **70**(2004), 115004 [arXiv:hep-ph/0406026 [hep-ph]]. H. C. Cheng and I. Low, *JHEP* **09**(2003), 051 [arXiv:hep-ph/0308199 [hep-ph]]. A. Birkedal, A. Noble, M. Perelstein and A. Spray, *Phys. Rev. D* **74**(2006), 035002 [arXiv:hep-ph/0603077 [hep-ph]]. S. Kanemura, S. Matsumoto, T. Nabeshima and N. Okada, *Phys. Rev. D* **82**(2010), 055026 [arXiv:1005.5651 [hep-ph]]. O. Lebedev, H. M. Lee and Y. Mambrini, *Phys. Lett. B* **707**, 570 (2012) [arXiv:1111.4482 [hep-ph]]. T. Abe, M. Kakizaki, S. Matsumoto and O. Seto, *Phys. Lett. B* **713**, 211 (2012) [arXiv:1202.5902 [hep-ph]]. Y. Farzan and A. R. Akbarieh, *JCAP* **10**(2012), 026 [arXiv:1207.4272 [hep-ph]]. J. M. Hyde, A. J. Long and T. Vachaspati, *Phys. Rev. D* **89**(2014), 065031 [arXiv:1312.4573 [hep-ph]]. P. Ko, W. I. Park and Y. Tang, *JCAP* **09**(2014), 013 [arXiv:1404.5257 [hep-ph]]. S. Baek, P. Ko, W. I. Park and E. Senaha, *JHEP* **05**, 036 (2013) [arXiv:1212.2131 [hep-ph]]. S. Baek, P. Ko and W. I. Park, *Phys. Rev. D* **90**(2014), no.5, 055014 [arXiv:1405.3530 [hep-ph]]. J. H. Yu, *Phys. Rev. D* **90**(2014), no.9, 095010 [arXiv:1409.3227 [hep-ph]]. C. R. Chen, Y. K. Chu and H. C. Tsai, *Phys. Lett. B* **741**, 205 (2015) [arXiv:1410.0918 [hep-ph]]. H. Zhang, C. S. Li, Q. H. Cao and Z. Li, *Phys. Rev. D* **82**(2010), 075003 [arXiv:0910.2831 [hep-ph]]. J. L. Diaz-Cruz and E. Ma, *Phys. Lett. B* **695**, 264 (2011) [arXiv:1007.2631 [hep-ph]]. S. Bhattacharya, J. L. Diaz-Cruz, E. Ma and D. Wegman, *Phys. Rev. D* **85**(2012), 055008 [arXiv:1107.2093 [hep-ph]]. T. Hambye and A. Strumia, *Phys. Rev. D* **88**(2013), 055022 [arXiv:1306.2329 [hep-ph]]. H. Davoudiasl and I. M. Lewis, *Phys. Rev. D* **89**(2014), no.5, 055026 [arXiv:1309.6640 [hep-ph]]. S. Baek, P. Ko and W. I. Park, *JCAP* **10**(2014), 067 [arXiv:1311.1035 [hep-ph]]. V. V. Khoze and G. Ro, *JHEP* **10**(2014), 061 [arXiv:1406.2291 [hep-ph]]. S. Fraser, E. Ma and M. Zakeri, *Int. J. Mod. Phys. A* **30**, no.03, 1550018 (2015) [arXiv:1409.1162 [hep-ph]]. A. Karam and K. Tamvakis, *Phys.*

- Rev. D **92**(2015), no.7, 075010 [arXiv:1508.03031 [hep-ph]]. T. Abe, M. Fujiwara, J. Hisano and K. Matsushita, JHEP **07**(2020), 136 [arXiv:2004.00884 [hep-ph]]. I
- [6] T. Hambye, JHEP **01**(2009), 028 [arXiv:0811.0172 [hep-ph]]. I, II, III, III
- [7] G. Arcadi, A. Djouadi and M. Raidal, Phys. Rept. **842**, 1 (2020) [arXiv:1903.03616 [hep-ph]]. III, III, V A, V A, V A
- [8] J. M. Cornwall, D. N. Levin and G. Tiktopoulos, Phys. Rev. D **10**(1974), 1145 [erratum: Phys. Rev. D **11**(1975), 972] B. W. Lee, C. Quigg and H. B. Thacker, Phys. Rev. D **16**(1977), 1519 B. W. Lee, C. Quigg and H. B. Thacker, Phys. Rev. Lett. **38**, 883 (1977) S. Kanemura, T. Kubota and E. Takasugi, Phys. Lett. B **313**, 155 (1993) [arXiv:hep-ph/9303263 [hep-ph]]. A. G. Akeroyd, A. Arhrib and E. M. Naimi, Phys. Lett. B **490**, 119 (2000) [arXiv:hep-ph/0006035 [hep-ph]]. J. Horejsi and M. Kladiva, Eur. Phys. J. C **46**, 81 (2006) [arXiv:hep-ph/0510154 [hep-ph]]. III
- [9] A. Arhrib, [arXiv:hep-ph/0012353 [hep-ph]]. III
- [10] G. Aad *et al.* [ATLAS], Phys. Rev. D **101**(2020), no.1, 012002 [arXiv:1909.02845 [hep-ex]].
- [11] M. Aaboud *et al.* [ATLAS], Phys. Rev. Lett. **122** (2019) no.23, 231801 [arXiv:1904.05105 [hep-ex]]. III, V A
- [12] [ATLAS], "Combination of searches for invisible Higgs boson decays with the ATLAS experiment," ATLAS-CONF-2020-052. III
- 1
- [13] A. M. Sirunyan *et al.* [CMS], Phys. Lett. B **793** (2019), 520-551 [arXiv:1809.05937 [hep-ex]]. 1
- [14] V. Khachatryan *et al.* [CMS], Phys. Rev. D **92**(2015), no.7, 072010 [arXiv:1507.06656 [hep-ex]]. III
- [15] M. Aaboud *et al.* [ATLAS], Phys. Lett. B **786**, 223 (2018) [arXiv:1808.01191 [hep-ex]]. III
- [16] E. Aprile *et al.* [XENON], JCAP **04** (2016), 027 [arXiv:1512.07501 [physics.ins-det]]. III, 6, V A
- [17] A. Falkowski, C. Gross and O. Lebedev, JHEP **05**(2015), 057 [arXiv:1502.01361 [hep-ph]]. III
- [18] M. Srednicki, R. Watkins and K. A. Olive, Nucl. Phys. B **310**, 693 (1988) E. W. Kolb and M. S. Turner, Front. Phys. **69**, 1 (1990) IV, IV
- [19] G. Aad *et al.* [ATLAS and CMS], $\sqrt{s} = 7$ and 8 TeV," JHEP **08**(2016), 045 [arXiv:1606.02266 [hep-ex]]. V A, V A, V A, V A
- [20] A. M. Sirunyan *et al.* [CMS], Phys. Rev. Lett. **121**, no.12, 121801 (2018) [arXiv:1808.08242 [hep-ex]]. V A
- [21] M. Aaboud *et al.* [ATLAS], Phys. Lett. B **786**, 59-86 (2018) [arXiv:1808.08238 [hep-ex]]. V A
- [22] A. M. Sirunyan *et al.* [CMS], Eur. Phys. J. C **79**, no.5, 421 (2019) [arXiv:1809.10733 [hep-ex]]. V A
- [23] M. Cepeda, S. Gori, P. Ilten, M. Kado, F. Riva, R. Abdul Khalek, A. Aboubrahim, J. Alimena, S. Alioli and A. Alves, *et al.* CERN Yellow Rep. Monogr. **7**, 221 (2019) [arXiv:1902.00134 [hep-ph]]. V A, V B, V B
- [24] G. Arcadi, A. Djouadi and M. Kado, Phys. Lett. B **805** (2020), 135427 [arXiv:2001.10750 [hep-ph]]. V A
- [25] J. Billard, L. Strigari and E. Figueroa-Feliciano, Phys. Rev. D **89** (2014) no.2, 023524 [arXiv:1307.5458 [hep-ph]]. 6
- [26] M. J. Dolan, C. Englert and M. Spannowsky, JHEP **10**, 112 (2012) [arXiv:1206.5001 [hep-ph]]. V B, V B, V B
- [27] A. Efrati and Y. Nir, [arXiv:1401.0935 [hep-ph]]. V B
- [28] J. Baglio, A. Djouadi, R. Gr  ber, M. M. M  CEhleitner, J. Quevillon and M. Spira, JHEP **04**, 151 (2013) [arXiv:1212.5581 [hep-ph]]. V B, V B
- [29] M. McCullough, Phys. Rev. D **90**, no.1, 015001 (2014) [erratum: Phys. Rev. D **92**, no.3, 039903 (2015)] [arXiv:1312.3322 [hep-ph]]. V B
- [30] M. Gorbahn and U. Haisch, JHEP **10**, 094 (2016) [arXiv:1607.03773 [hep-ph]].
- [31] F. Maltoni, D. Pagani, A. Shivaji and X. Zhao, Eur. Phys. J. C **77**, no.12, 887 (2017) [arXiv:1709.08649 [hep-ph]]. V B
- [32] G. D. Kribs, A. Maier, H. Rzehak, M. Spannowsky and P. Waite, Phys. Rev. D **95**, no.9, 093004 (2017) [arXiv:1702.07678 [hep-ph]].
- [33] The ATLAS collaboration [ATLAS Collaboration], ATLAS-CONF-2021-016. V B
- [34] L. B. Chen, H. T. Li, H. S. Shao and J. Wang, JHEP **03**, 072 (2020) [arXiv:1912.13001 [hep-ph]]. V B, 9, V B, VI
- [35] A. J. Barr, M. J. Dolan, C. Englert and M. Spannowsky, Phys. Lett. B **728**, 308-313 (2014) [arXiv:1309.6318 [hep-ph]]. V B, V B
- [36] Q. Li, Q. S. Yan and X. Zhao, Phys. Rev. D **89**, no.3, 033015 (2014) [arXiv:1312.3830 [hep-ph]]. V B
- [37] Q. H. Cao, B. Yan, D. M. Zhang and H. Zhang, Phys. Lett. B **752**, 285-290 (2016) [arXiv:1508.06512 [hep-ph]].
- [38] Q. Li, Z. Li, Q. S. Yan and X. Zhao, Phys. Rev. D **92**, no.1, 014015 (2015) [arXiv:1503.07611 [hep-ph]].
- [39] Q. H. Cao, Y. Liu and B. Yan, Phys. Rev. D **95**, no.7, 073006 (2017) [arXiv:1511.03311 [hep-ph]].
- [40] Q. H. Cao, G. Li, B. Yan, D. M. Zhang and H. Zhang, Phys. Rev. D **96**, no.9, 095031 (2017) [arXiv:1611.09336 [hep-ph]].
- [41] H. J. He, J. Ren and W. Yao, Phys. Rev. D **93**, no.1, 015003 (2016) [arXiv:1506.03302 [hep-ph]].
- [42] T. Huang, J. M. No, L. Perni  , M. Ramsey-Musolf, A. Safonov, M. Spannowsky and P. Winslow, Phys. Rev. D **96**, no.3, 035007 (2017) [arXiv:1701.04442 [hep-ph]].
- [43] C. T. Lu, J. Chang, K. Cheung and J. S. Lee, JHEP **08**, 133 (2015) [arXiv:1505.00957 [hep-ph]].

- [44] A. Papaefstathiou, L. L. Yang and J. Zurita, *Phys. Rev. D* **87**, no.1, 011301 (2013) [arXiv:1209.1489 [hep-ph]].
- [45] J. H. Kim, K. Kong, K. T. Matchev and M. Park, *Phys. Rev. Lett.* **122**, no.9, 091801 (2019) [arXiv:1807.11498 [hep-ph]].
- [46] G. Buchalla, M. Capozzi, A. Celis, G. Heinrich and L. Scyboz, *JHEP* **09**, 057 (2018) [arXiv:1806.05162 [hep-ph]].
- [47] J. H. Kim, M. Kim, K. Kong, K. T. Matchev and M. Park, *JHEP* **09**, 047 (2019) [arXiv:1904.08549 [hep-ph]].
- [48] G. Li, L. X. Xu, B. Yan and C. P. Yuan, *Phys. Lett. B* **800**, 135070 (2020) [arXiv:1904.12006 [hep-ph]].
- [49] J. Chang, K. Cheung, J. S. Lee, C. T. Lu and J. Park, *Phys. Rev. D* **100**, no.9, 096001 (2019) [arXiv:1804.07130 [hep-ph]].
- [50] M. Abdughani, D. Wang, L. Wu, J. M. Yang and J. Zhao, [arXiv:2005.11086 [hep-ph]]. V B, V B
- [51] R. Contino, D. Curtin, A. Katz, M. L. Mangano, G. Panico, M. J. Ramsey-Musolf, G. Zanderighi, C. Anastasiou, W. Astill and G. Bambhaniya, *et al.* CERN Yellow Rep., no.3, 255-440 (2017) [arXiv:1606.09408 [hep-ph]]. V B
- [52] D. GonÁsalves, T. Han, F. Kling, T. Plehn and M. Takeuchi, *Phys. Rev. D* **97**, no.11, 113004 (2018) [arXiv:1802.04319 [hep-ph]]. V B
- [53] K. Fujii, C. Grojean, M. E. Peskin, T. Barklow, Y. Gao, S. Kanemura, H. Kim, J. List, M. Nojiri and M. Perelstein, *et al.* [arXiv:1710.07621 [hep-ex]]. V B
- [54] J. de Blas, M. Cepeda, J. D'Hondt, R. K. Ellis, C. Grojean, B. Heinemann, F. Maltoni, A. Nisati, E. Petit and R. Rattazzi, *et al.* *JHEP* **01**, 139 (2020) [arXiv:1905.03764 [hep-ph]]. V B
- [55] K. Fujii, C. Grojean, M. E. Peskin, T. Barklow, Y. Gao, S. Kanemura, H. D. Kim, J. List, M. Nojiri and M. Perelstein, *et al.* [arXiv:1506.05992 [hep-ex]]. V B
- [56] J. Braathen and S. Kanemura, *Eur. Phys. J. C* **80**, no.3, 227 (2020) [arXiv:1911.11507 [hep-ph]]. V B, V B
- [57] P. Roloff *et al.* [CLICdp], [arXiv:1901.05897 [hep-ex]]. V B, V B
- [58] H. Abramowicz, A. Abusleme, K. Afanaciev, N. A. Tehrani, C. BalÁzs, Y. Benhammou, M. Benoit, B. Bilki, J. J. Blaising and M. J. Boland, *et al.* *Eur. Phys. J. C* **77**, no.7, 475 (2017) [arXiv:1608.07538 [hep-ex]].
- [59] P. N. Burrows *et al.* [CLICdp and CLIC], [arXiv:1812.06018 [physics.acc-ph]].
- [60] S. Kanemura, S. Kiyoura, Y. Okada, E. Senaha and C. P. Yuan, *Phys. Lett. B* **558**, 157-164 (2003) [arXiv:hep-ph/0211308 [hep-ph]]. V B
- [61] S. Kanemura, Y. Okada, E. Senaha and C. P. Yuan, *Phys. Rev. D* **70**, 115002 (2004) [arXiv:hep-ph/0408364 [hep-ph]]. V B
- [62] A. Ahriche, A. Arhrib and S. Nasri, *JHEP* **02**(2014), 042 [arXiv:1309.5615 [hep-ph]]. V B
- [63] G. J. Gounaris, D. Schildknecht and F. M. Renard, *Phys. Lett. B* **83**, 191 (1979) V B
- [64] V. D. Barger, T. Han and R. J. N. Phillips, *Phys. Rev. D* **38**(1988), 2766 V C
- [65] V. A. Ilyin, A. E. Pukhov, Y. Kurihara, Y. Shimizu and T. Kaneko, *Phys. Rev. D* **54**(1996), 6717 [arXiv:hep-ph/9506326 [hep-ph]].
- [66] A. Djouadi, W. Kilian, M. Muhlleitner and P. M. Zerwas, *Eur. Phys. J. C* **10**, 27-43 (1999) [arXiv:hep-ph/9903229 [hep-ph]]. V C
- [67] J. Tian, K. Fujii and Y. Gao, [arXiv:1008.0921 [hep-ex]].
- [68] F. Boudjema and E. Chopin, *Z. Phys. C* **73**, 85 (1996) [arXiv:hep-ph/9507396 [hep-ph]]. V C
- [69] V. D. Barger and T. Han, *Mod. Phys. Lett. A* **5**, 667 (1990)
- [70] A. Dobrovolskaya and V. Novikov, *Z. Phys. C* **52**, 427 (1991)
- [71] A. Abbasabadi, W. W. Repko, D. A. Dicus and R. Vega, *Phys. Rev. D* **38**(1988), 2770
- [72] E. W. N. Glover and J. J. van der Bij, *Nucl. Phys. B* **309**, 282 (1988) V C
- [73] T. Plehn, M. Spira and P. M. Zerwas, *Nucl. Phys. B* **479**, 46 (1996) [erratum: *Nucl. Phys. B* **531**, 655 (1998)] [arXiv:hep-ph/9603205 [hep-ph]]. V C
- [74] S. Dawson, S. Dittmaier and M. Spira, *Phys. Rev. D* **58**(1998), 115012 [arXiv:hep-ph/9805244 [hep-ph]].
- [75] M. Spira, [arXiv:hep-ph/9510347 [hep-ph]]. V C
- [76] [ATLAS], ATLAS-CONF-2021-009.
- [77] G. Aad *et al.* [ATLAS], *Phys. Rev. D* **102** (2020), 112006 [arXiv:2005.12236 [hep-ex]]. V C
- [78] M. Aaboud *et al.* [ATLAS], *Phys. Lett. B* **782** (2018), 750-767 [arXiv:1803.11145 [hep-ex]]. V C
- [79] A. Ahriche *et al.*, in preparation. V C

V C